Pebble abrasion during fluvial transport: Experimental results and implications for the evolution of the sediment load along rivers

Pebble abrasion during fluvial transport: Experimental results and implications for the evolution of the sediment load along rivers

Mikaël Attal[1] and Jérôme Lavé[2]

Received 30 March 2009; revised 18 August 2009; accepted 2 September 2009; published 15 December 2009.

[1] In actively eroding landscapes, fluvial abrasion modifies the characteristics of the sediment carried by rivers and consequently has a direct impact on the ability of mountain rivers to erode their bedrock and on the characteristics and volume of the sediment exported from upland catchments. In this experimental study, we use a novel flume replicating hydrodynamic conditions prevailing in mountain rivers to investigate the role played by different controlling variables on pebble abrasion during fluvial transport. Lithology controls abrasion rates and processes, with differences in abrasion rates exceeding two orders of magnitude. Attrition as well as breaking and splitting are efficient processes in reducing particle size. Mass loss by attrition increases with particle velocity but is weakly dependent on particle size. Fragment production is enhanced by the use of large particles, high impact velocities and the presence of joints. Based on our experimental results, we extrapolate a preliminary generic relationship between pebble attrition rate and transport stage (τ^*/τ_c^*), where τ^* = fluvial Shields stress and τ_c^* = critical Shields stress for incipient pebble motion. This relationship predicts that attrition rates are independent of transport stage for (τ^*/τ_c^*) ≤ 3 and increase linearly with transport stage beyond this value. We evaluate the extent to which abrasion rates control downstream fining in several different natural settings. A simplified model predicts that the most resistant lithologies control bed load flux and fining ratio and that the concavity of transport-limited river profiles should rarely exceed 0.25 in the absence of deposition and sorting.

Citation: Attal, M., and J. Lavé (2009), Pebble abrasion during fluvial transport: Experimental results and implications for the evolution of the sediment load along rivers, *J. Geophys. Res.*, *114*, F04023, doi:10.1029/2009JF001328.

1. Introduction

[2] Mountainous landscapes result from the competition between rock uplift and erosion. In nonglaciated regions, rivers have been recognized as one of the primary agents of erosion. During mountain denudation, river networks play a dual role. First, rivers incise into bedrock and thus drive gravitational instabilities and landslides, controlling in that way part of the hillslope erosion processes [e.g., *Burbank et al.*, 1996; *Whipple et al.*, 1999]. Second, rivers convey the erosion products supplied from hillslopes and from upstream to sedimentary basins. Mountain rivers transport the erosion products as dissolved load, suspended load and bed load. Bed load characteristics, i.e., pebble size distribution, lithologic proportion and ratio to total exported load, usually vary along a river course from its source down to the foreland basins. This longitudinal evolution depends on the geographic distribution of sediment fluxes from hillslopes, on the characteristics of these sources of sediment, on the abrasion processes during fluvial transport, and on the hydraulic sorting processes during fluvial transport [*Attal and Lavé*, 2006].

[3] There are at least two reasons why such downstream evolution of sediment size and quantity needs to be addressed, understood and quantified. First, an appropriate theory and quantification of this phenomenon would provide the framework to interpret preserved sedimentary records of erosion in detrital series. In particular, it would help to unravel the paleoclimatic or tectonic information related to the denuded orogen by correcting the sedimentary signal from the distortion that abrasion and fluvial transport processes may introduce between the internal mountainous sediment source and the foreland basin. Second, researchers are increasingly recognizing the potentially important role of sediment flux, in particular bed load flux, in determining river incision rates into bedrock [*Gilbert*, 1877; *Willgoose et al.*, 1991; *Howard et al.*, 1994; *Sklar and Dietrich*, 1998, 2004; *Whipple and Tucker*, 2002; *Cowie et al.*, 2008]. Because river incision controls landscape denudation in active orogens, quantifying the downstream evolution of the sediment load is a central issue in long-term landscape evolution models and related problems, such as the linkages between climate, erosion, and tectonics.

[4] For more than a century, scientists have studied the evolution of bed load characteristics during fluvial transport. The rounding processes that transform angular clasts at

[1]School of GeoSciences, University of Edinburgh, Edinburgh, UK.
[2]Centre de Recherches Pétrographiques et Géochimiques, Nancy, France.

0148-0227/09/2009JF001328

the source to rounded pebbles with varied shapes received considerable attention during the first half of the 20th century [e.g., *Wentworth*, 1919; *Krumbein*, 1941; *Kuenen*, 1956] and a general consensus has arisen on the qualitative description of this rounding phenomenon. In contrast, the nature of the processes that lead to downstream size reduction has been debated for more than 50 years. The controversy arises from the general discrepancy between size reduction rates measured in experimental studies of pebble abrasion and the downstream fining rates measured along rivers [*Kuenen*, 1956; *Bradley*, 1970; *Shaw and Kellerhals*, 1982; *Kukal*, 1990; *Brewer and Lewin*, 1993; *Kodama*, 1994a, 1994b]. Downstream fining in rivers is commonly described by *Sternberg*'s [1875] law:

$$D = D_0.e^{-\delta L t}, \quad (1)$$

where D_0 = initial grain size, D = grain size after a traveled distance L_t, and δ = fining rate in km^{-1}. Experimental size reduction rates have been found to be one to two orders of magnitude lower than fining rates in the field. This discrepancy has led several authors to conclude that selective sorting during fluvial transport is the dominant control on downstream sediment grain size reduction [*Brierley and Hickin*, 1985; *Paola et al.*, 1992; *Brewer and Lewin*, 1993; *Ferguson et al.*, 1996; *Surian*, 2002; *Moussavi-Harami et al.*, 2004]. Such a conclusion is probably valid in river systems where sediment aggradation is occurring (e.g., alluvial rivers). In contrast, in a river system which is not aggrading, selective sorting can be expected to be minimal because there is no selective deposition of coarse material. Other authors have thus proposed that the discrepancy results from higher abrasion rates in natural systems than in experimental conditions, either because of the combined roles of chemical weathering and abrasion [*Bradley*, 1970; *Jones and Humphrey*, 1997] or because most of the experimental devices improperly reproduce pebble trajectories and associated impacts [e.g., *Kuenen*, 1956; *Mikos and Jaeggi*, 1995; *Lewin and Brewer*, 2002]. This latter criticism is mainly aimed at the tumbling barrels used in many previous studies (e.g., *Daubrée* [1879], *Wentworth* [1919], *Krumbein* [1941], *Brewer and Lewin* [1993], *Mikos and Jaeggi* [1995], and *Jones and Humphrey* [1997]; see exhaustive list in the work by *Lewin and Brewer* [2002]), although some of them were designed to replicate high velocity impacts characterizing mountain rivers [*Kodama*, 1994b].

[5] The purpose of the present study is to characterize and quantify pebble abrasion during fluvial transport using a novel experimental device that reproduces for the first time both the type and magnitude of hydrodynamic conditions prevailing during floods in mountain rivers [*Attal et al.*, 2006]. In this parametric study, we explore the dependence of abrasion on controlling variables: sediment amount, particle velocity, size, and lithology, and channel floor conditions. Our facility consists of a circular flume in which a flow is produced by four tangential water injection points (Figure 1). Particular attention was given to the possibility of measuring the hydrodynamic variables and pebble trajectories in order to enable transposition of the results to natural rivers. After a detailed description of the flume and of the procedure applied to measure hydrodynamic variables, abrasion rates and the characteristics of abrasion products, we present our experimental results of pebble abrasion by interpebble impacts and describe the controls exerted by the above variables on abrasion rates. Finally, we consider the implications of our results for the evolution of the bed load during its journey along fluvial networks and discuss the effects of this evolution on fluvial erosion, on landscape evolution and on the information recorded in the characteristics of detrital rocks along rivers and in sedimentary basins.

2. Experimental Device and Procedure

2.1. Experimental Device

[6] Two different types of device that permit sediments to be transported over large distances have been used to study pebble abrasion: tumbling mills and circular flumes. In contrast with tumbling mills, in which abrasion is a combination of intergranular friction and rolling during sediment motion and for which traveling distance is difficult to estimate [*Mikos and Jaeggi*, 1995], circular flumes offer the possibility to better reproduce the hydrodynamic conditions prevalent in natural rivers, because sediment motion is induced by a water current. In the first design of circular flume proposed by *Kuenen* [1956], water circulation was maintained by paddles in rotation. However, such a paddle system may generate unrealistic turbulence at the edges of each paddle; it also creates difficulties to monitor variables or to introduce sensors and instruments into the flume; finally, interactions between pebbles and paddles cannot be excluded, in particular at high flow. Alternative designs that prevent such drawbacks involve circular flow sustained by lateral fluid injection and a water recirculation system [*Lewin and Brewer*, 2002; *Attal et al.*, 2006].

[7] In the water recirculating device that we developed [*Attal et al.*, 2006], the water is entrained by a 22 kW pump. The pump system is driven by a flowmeter that allows the discharge to be adjusted to any value between 0 and 140 l/s. Water is brought to the circular flume by flexible pipes and is injected tangentially at four points to provide an approximately uniform flow within the flume (Figure 1). The stainless steel circular flume has the following dimensions: external diameter = 1.5 m, flume width = 0.3 m and flume depth = 0.6 m. Water is evacuated by overflowing the internal wall of the flume and is collected in a 5 m^3 tank before being recirculated by the pump. During experiments, a vortex is created by the effect of the centrifugal force exerted on the water column. The bed of the flume is protected by removable plates which can be covered by different kinds of material. To study pebble abrasion by impacts between moving pebbles without the influence of bedrock (this study), ''nonabrasive'' plates covered with pieces of tires were installed on the flume floor. To study interactions between pebble and bedrock, or between moving pebble and immobile pebbles, ''nonabrasive'' plates can be replaced by ''abrasive'' plates with varied roughness and strength. A 0.5 mm mesh sieve is located between the flume and the tank to collect the largest abrasion products and to prevent damage to the pump.

[8] For some experiments and to investigate scaling issues, a simplified and reduced (1/5 scale) version of the above device was used (Figure 1d). In this device, hereafter

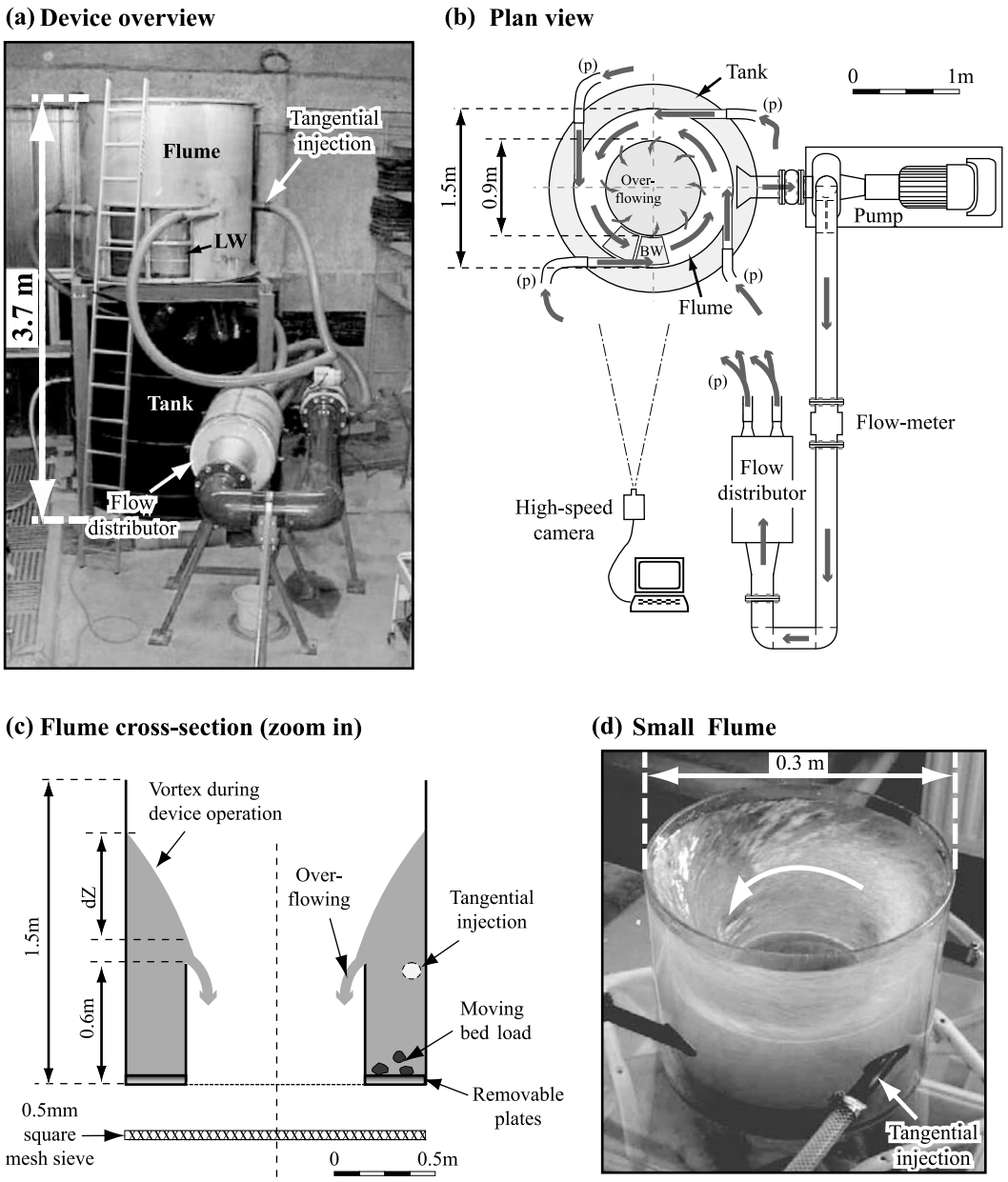

Figure 1. The experimental device. Basal and lateral windows (BW and LW, respectively) allow the visualization of pebble motion during experiments. (a) Photo of the device. (b) Plan view of the device. For clarity, the pipes connecting the flow distributor to the flume (p) have not been drawn. (c) Cross section of the flume showing the vortex created by the fluid in rotation during experiments (zoom $\times 2$ with respect to Figure 1b). (d) Photo of the small circular flume (1/5 scale) showing the vortex.

called the small flume, four similar pumps provide constant tangential injection discharge directly in the flume channel. Hydraulic and pebble transport conditions are consistent with those prevailing in the large flume [*Attal*, 2003].

2.2. Flow Dynamics and Particle Behavior

[9] Despite its circular geometry, the experimental device reproduces flow patterns and particle behavior similar to those described in natural rivers [*Attal et al.*, 2006], in experimental straight flumes or in numerical models [e.g., *Niño et al.*, 1994; *Niño and García*, 1994]. Using the height of the vortex, mean water velocity can easily be determined for any experiment. For a radially uniform flow, the vortex size depends on the mean water velocity across the flume [*Chang*, 1988; *Attal et al.*, 2006]:

$$dZ \approx \frac{wU_{fl}^2}{gr_m}, \tag{2}$$

where dZ is the height difference between the top and the bottom of the vortex (Figure 1c), w is the flume width, U_{fl} is the mean water velocity across a flume section, g is the gravitational acceleration and r_m is the mean radius of the flume. In this flume, the height of the external wall (1.5 m) limits the maximum average flow velocity to $\sim$4 m.s^{-1}. The

average flow velocity depends on the injection velocity and on the bed roughness. Roughness increases with an increase in size and/or amount of sediment and it controls the vertical and radial gradients of fluid velocity [*Attal et al.*, 2006]. The tangential velocity is relatively constant in a vertical profile, except near the floor where an abrupt velocity drop marks the basal boundary layer, whose thickness increases with sediment roughness. The application of the Euler theorem allows the calculation of the basal shear stress exerted on the flume floor and on the pebbles [*Attal et al.*, 2006]. Along a radial profile, the tangential velocity is also relatively constant when the roughness is low or for high fluid injection. However, a radial gradient characterized by a decrease in velocity from the outer wall to the inner wall of the flume may appear when roughness is large. In that case, equation (2) reduces the radius-averaged velocity to a crude approximation [*Attal et al.*, 2006].

[10] The flume lateral and basal windows (LW and BW in Figures 1a and 1b) allow observation of particle behavior. Particle trajectories and collisions were recorded and analyzed using a high-speed camera. When drag and lift forces are sufficient to extract pebbles from their position, pebbles move by saltation and occasionally by rolling (Figure 2a). Mean saltation velocity u_p during a hop, as well as trajectory, were measured directly from particle tracking on the movies (1/125 s time sampling). In order to accurately calculate the average traveling velocity U_p and the mean distance traveled by the pebbles during an experiment, the average radius of curvature of the particle trajectory was estimated. This radius is a function of the centrifugal force acting on the particle, a centripetal force due to the combined effects of a radial pressure gradient and of secondary currents existing in the basal boundary layer [e.g., *Chang*, 1988], and the momentum transfer during interparticle collision and collision with the walls of the flume. For the range of pebble sizes and flow velocities used in this study, it was observed through the basal window that pebbles occupy the full width of the flume but that the mean curvature radius and average particle path slightly vary, depending on pebble size, velocity and amount of sediment (Figure 2b).

[11] The average traveling velocity U_p to accomplish a round trip in the flume was determined by dividing the mean distance traveled by the pebbles during a lap by the mean time required by the pebbles to accomplish a lap. This time was estimated in three different ways: by timing a painted pebble during the experiment; by timing a specific pebble (specific in shape and/or color) that was recognizable on the video record, and by estimating the flux of pebbles on the video record and then dividing it by the number of pebbles introduced into the flume. The three methods provide similar results and the average velocity U_p is found to be very close to the mean hop velocity u_p, except at low stage, when pebble motion is only partial. In this latter case, the average traveling velocity U_p represents the sum of motion periods characterized by a velocity u_p and of resting

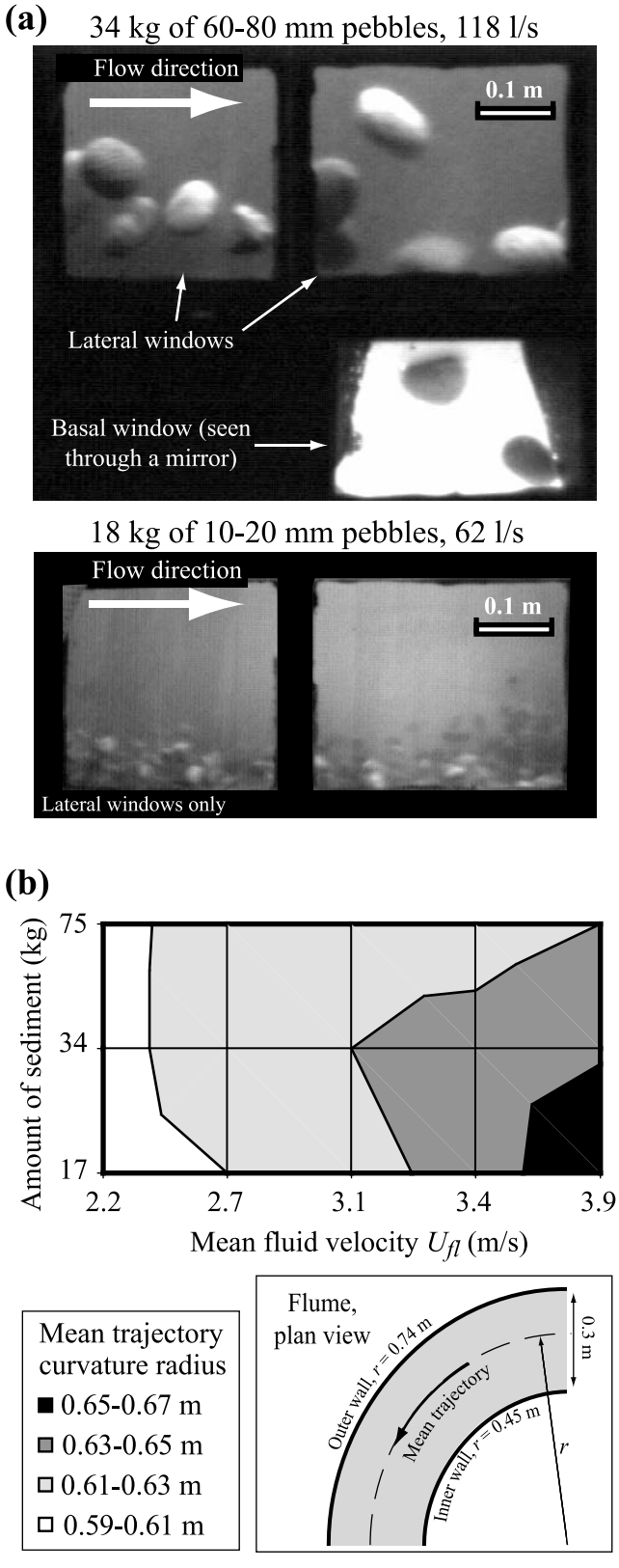

Figure 2. (a) Snapshots of movies recorded with a high speed camera to track the trajectories of pebbles in saltation during experiments with (top) 34 kg of 60–80 mm pebbles and an input discharge of 118 l/s and (bottom) 18 kg of 10–20 mm pebbles and an input discharge of 62 l/s. (b) Mean trajectory curvature radius as a function of fluid velocity and sediment amount for the 60–80 mm pebbles. Trajectories with large curvature radius are observed for high velocity and low sediment amount.

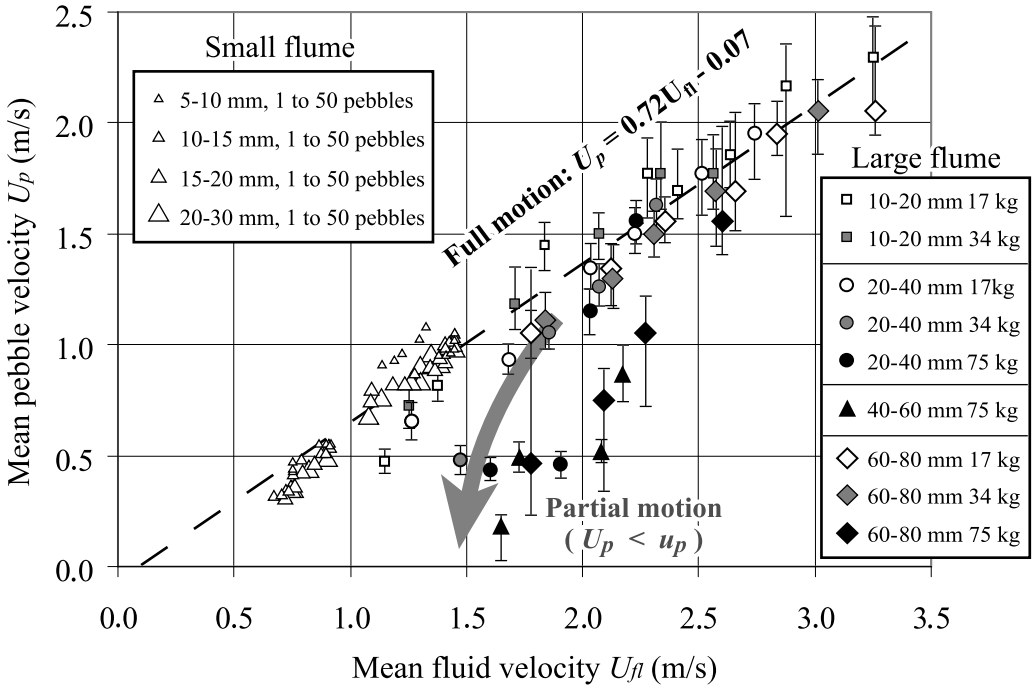

Figure 3. Mean pebble velocity during a round trip as a function of mean water velocity in the flumes. Both small and large flume data describe a linear relationship at full motion. For low velocity and/or large amount of sediments, data depart from the trend, because round trips include both motion and resting periods. Particle velocities are obtained using three different methods (see text); average values (data points) and maximum and minimum values (tips of "error" bars) are shown.

periods; in this case, we frequently observed that some particles remain permanently motionless. For both flumes, the mean pebble velocity is, to a first approximation, linearly related to the water velocity (Figure 3) almost whatever the size and quantity of sediments introduced in the flume, as long as the sediments are in full motion. This "full motion" condition was fulfilled in almost all of our abrasion experiments.

2.3. Experimental Procedure

[12] For most of the experiments (except multilithology experiments), limestone pebbles were used. Such lithology is sufficiently "soft" to obtain significant abrasion rates even for short experiment durations. All the limestone pebbles were collected in a single gravel bar located in Aspremont, along the Grand Buëch River (Dévoluy-Bochaine Massif, French Alps). Most of the pebbles in the river are sourced from Upper Jurassic and Cretaceous fine-grained limestones, and have traveled at least 10 km. This enabled us to use relatively well-rounded and non-weathered clasts, in order to avoid an overestimation of the abrasion rates due to the fast rounding of angular clasts [*Krumbein*, 1941; *Kuenen*, 1956; *Pearce*, 1971] or to the removal of the weakened superficial layer of weathered pebbles [*Bradley*, 1970]. Well-sorted material was used in the experiments, and four size classes were defined: 10–20 mm, 20–40 mm, 40–60 mm and 60–80 mm. These dimensions correspond to the mesh of the square mesh sieves used to sort the sediment. Gravel of size varying between 10 and 28 mm was also collected for experiments in the small flume.

[13] Pebble abrasion during fluvial transport results from moving pebbles impacting other moving pebbles or "substrate" (bedrock or immobile pebbles). In order to isolate a single process and better characterize the control exerted by the different variables on abrasion, our experiments mostly focus on abrasion by impacts between moving pebbles. To do so, we used rubber flooring to suppress any substrate abrasion and conducted our experiments primarily at full transport stage, i.e., with all the pebbles in motion. At full transport stage, water and pebble velocities were found to be approximately radially uniform, thus enabling a simpler interpretation to our parametric study. Four sets of experiments were performed in both flumes (Table 1) to investigate the influence of different variables on pebble abrasion rate: amount of sediment, particle velocity, size and lithology, and bed conditions. One specific set of experiments was also performed in the small flume with varying bed conditions to document the effect of the impacts with immobile pebbles. Experiment duration ranged between 0.5 and 2 h in the large flume and between 1.5 and 7 h in the small flume. At the end of each experiment, all pebbles and fragments were collected from the flume and from the 0.5 mm square mesh sieve located between the flume and the tank. The amount of abrasion was measured by sieving into size classes and weighing all the sediment before and after each experiment. A standard drying procedure was applied before any weighing; this minimized the empirical error due to wetness differences to <5% for both small and large flume experiments, as estimated from replicating the weighing procedure on the same sediment sample.

[14] Abrasion rates E_t and E_d are expressed in percent mass loss per unit time and per unit traveled distance

Table 1. Description of the Four Sets of Experiments

	Large Flume		Small Flume	
	Set 1	Set 2	Set 3	Set 4
Tested variable	grain size (well sorted material), flow and particle velocity, amount of sediment, study of the abrasion products	lithology	heterogeneity in grain size	bed condition, amount of sediment
Number of runs	50	2	2 + 3 repeat. tests	11 + 3 repeat. tests
Bed conditions	nonabrasive	nonabrasive	nonabrasive	variable
Material grain size	well sorted: 10–20 mm (subset 1a, 23 runs), 20–40 mm (subset 1b, 17 runs), 40–60 and 60–80 mm (subset 1c, 10 runs)	well sorted: 40–80 mm	poorly sorted: individual limestone gravel of different size (9 to 39 mm) diluted in ~400 g of 11–18 mm or 18–30 mm granitic gravel	well sorted: 10–20 mm
Input discharge	variable	constant (97 l/s)	constant (4 × 0.4 l/s)	constant (4 × 0.4 l/s)
Amount of sediment	variable	constant (75 kg)	constant (~500–650 g)	variable
Lithology	homogeneous (limestone)	variable: 15 kg of pebbles with varied lithologies + 60 kg of granitic pebbles)	individual limestone gravel + 400 g of granitic gravel	homogeneous (limestone)

respectively ($E_d = E_t/U_p$). Abrasion rates are calculated following

$$E_d = ln(m_0/m)/L_t \quad (3)$$

(obtained by integrating equation (1) and assuming that E_d does not vary during the experiment), where m_0 = initial pebble mass and m = pebble mass after a traveled distance L_t; note that because particle mass scales with D^3, it can be shown by combining equations (1) and (3) that an abrasion rate E_d corresponds to a size reduction coefficient $\delta = E_d/3$. When estimating the mass loss rate per unit traveled distance, the error associated with the methods used to determine pebble weight and velocity ranges between 10 and 30% at high and low transport stage respectively [*Attal*, 2003].

[15] Different abrasion processes produce different types of products [*Kuenen*, 1956; *Kodama*, 1994b]: clay, silt and sand are produced by attrition (the action of pebbles rubbing against each other) and crushing, while small and large fragments are produced by splitting, breaking and chipping. No quantitative definition, based for example on fragment size or morphology, has been proposed so far to identify the above distinct mass loss processes. In the following, we will therefore arbitrarily assume that the fragments produced by splitting, chipping and breaking processes are larger than sand size, i.e., the 0.5–1 mm fraction, and are intercepted by the 0.5 mm mesh sieve. All the abrasion products that pass through the sieve and settle down the tank at the end of the experiments will be considered as attrition and crushing products. We define the abrasion rate as the total mass loss rate including both fragments and fine products. The term attrition rate is reserved for the production rate of the finest fraction (<0.5 mm), while the term fragment production rate refers to the production rate of fragments larger than 0.5 mm.

2.4. Experiment Reproducibility

[16] To test the reproducibility of our results, several experiments were replicated with similar hydrodynamic conditions and sediment amounts (Figure 4). The abrasion rates obtained for these experiments were found to be consistent within error, with differences in abrasion rates typically ranging between 5 and 20%. These differences result mostly from the variation in sediment geometry and mechanical characteristics from experiment to experiment. The same sediment was used in more than one experiment, with variable addition of ''fresh'' material. Successive experiments tend to further round pebbles, leading to a potential decrease in abrasion rate [*Kuenen*, 1956]. In addition, the sediment used was sampled on a natural gravel bar and was thus not perfectly homogeneous: the least resistant pebbles are probably abraded away during successive experiments, causing the remaining material to become more resistant and thus leading to a general decrease in total abrasion rate. For example, four experiments were conducted with ~34 kg of 10–20 mm pebbles and a mean pebble velocity of 1.8 m/s (Figure 4c): the first three experiments were carried out in a row using initially fresh material and produced consistent abrasion rates with a relative deviation of 8%; in contrast, the fourth experiment was carried out using sediment that had experienced 20 runs (but including a ~15% addition of fresh material) and produced an abrasion rate 26% lower than the mean value obtained in the first 3 experiments. Such a deviation can probably be viewed as a maximum estimate of the variability that can be expected for our experiments, as the same sediment was never used for more than 20 runs. Finally, it has to be noted that differences between replicates were found to increase with pebble size and velocity and with the rate of fragment production.

3. Experimental Results

3.1. Amount of Sediment and Abrasion Rates

[17] The amount of sediment introduced into the flume is expected to have a significant influence on pebble abrasion rate by controlling the frequency of impacts. Initially, one experiment was carried out with only six 20–40 mm pebbles (~350 g of material) to make sure that the tire floor fulfills the condition of nonabrasivity. The pebbles traveled at a mean velocity of ~2 m/s for 12 h. The pebble

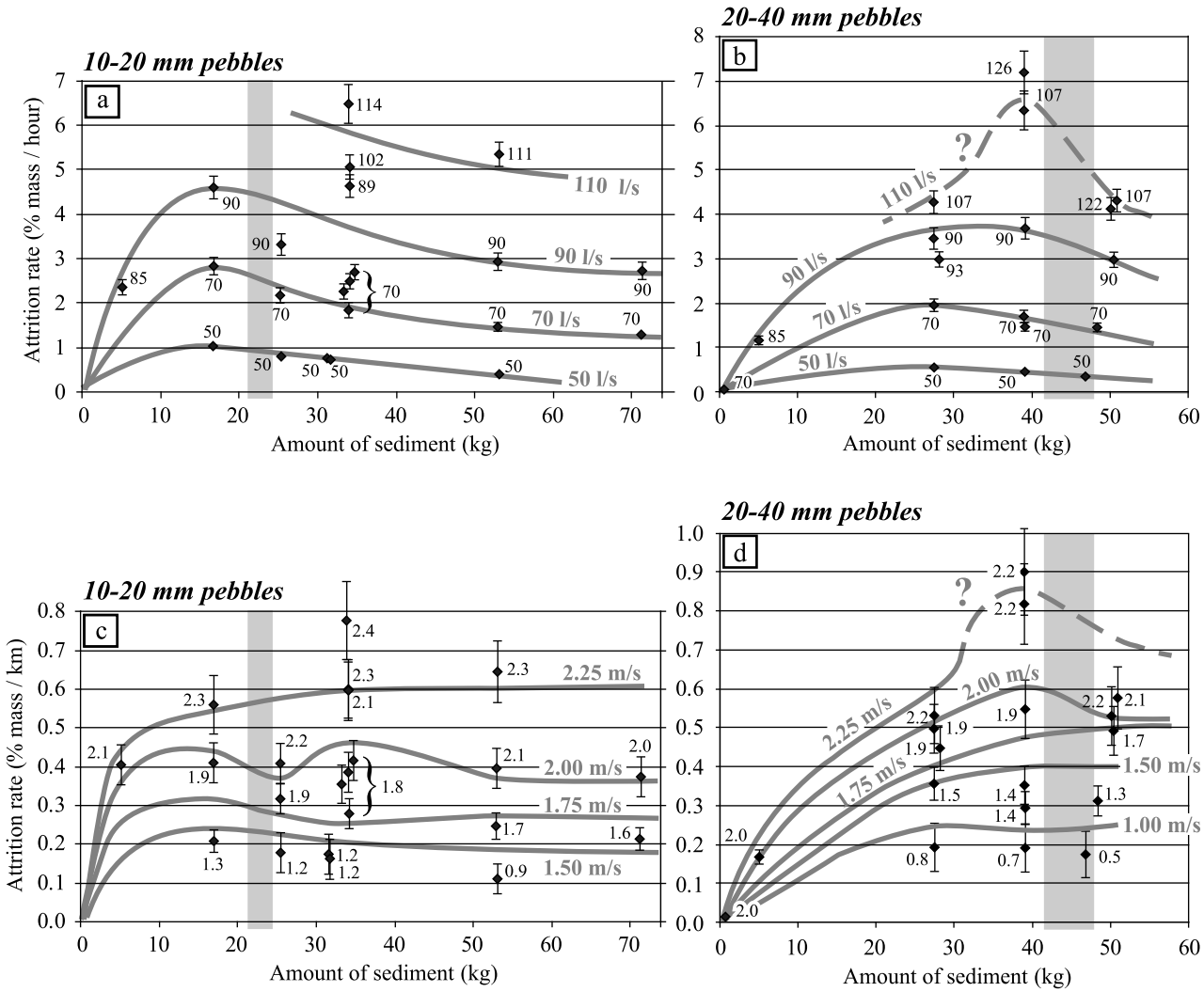

Figure 4. Attrition rate as a function of the amount of sediment introduced into the flume for (a, c) 10–20 mm and (b, d) 20–40 mm pebbles. Gray zone indicates the approximate amount of sediment for which the floor of the flume is fully covered with pebbles (packing density is p_{cp}; see text). In Figures 4a and 4b attrition rate is in % mass per hour; water discharge (in l/s) is indicated on data points and on extrapolated curves for constant water discharge. Discharges of 50, 70, and 90 l/s correspond to fluid injection velocities of 2.5, 3.5, and 4.5 m/s, respectively. In Figures 4c and 4d attrition rate is in % mass per km; mean pebble velocity (in m/s) is indicated on data points and on extrapolated curves for constant pebble velocity.

abrasion rate did not exceed 0.08 percent mass loss per hour, i.e., less than ~1/20 of the mass loss measured in similar hydrodynamic conditions but for large amount of sediments. This very low abrasion rate is explained by a very low probability of collision and confirms the non-abrasivity of the flume floor and walls.

[18] In order to interpret the results of experiments involving various amounts of pebbles, we introduce the quantity of sediment in terms of packing density on the flume floor. This packing density can be expressed as

$$p = S_e/A_f = n_p \pi D^2/4A_f = 3M_s/2\rho_s D A_f, \qquad (4)$$

considering that pebbles are spheres of diameter D, with S_e = the projected surface of the pebbles, A_f = total area of the flume floor (1.08 m^2 for the large flume), n_p = number of pebbles introduced in the flume, M_s = mass of sediment introduced into the flume, and ρ_s = rock density (~2650 kg/m^3 here). Depending on the packing model (square or hexagonal packing), the packing density p_{cp} to fully cover a surface with contiguous spheres ranges between $\pi/4 \le p_{cp} \le \pi/2\sqrt{3}$. Using the geometric mean of the grain sizes for each class, the close packing mass required to cover the floor of the large flume M_{sc} is 21–24 kg for the 10–20 mm pebbles, 42–48 kg for the 20–40 mm pebbles, 74–85 kg for the 40–60 mm pebbles and 104–119 kg for the 60–80 mm pebbles. Despite the presence of the flume walls and the simplifying assumption that pebbles are spherical, the direct measurement of the actual masses of sediment required to roughly cover the floor of the flume corroborates the model estimates.

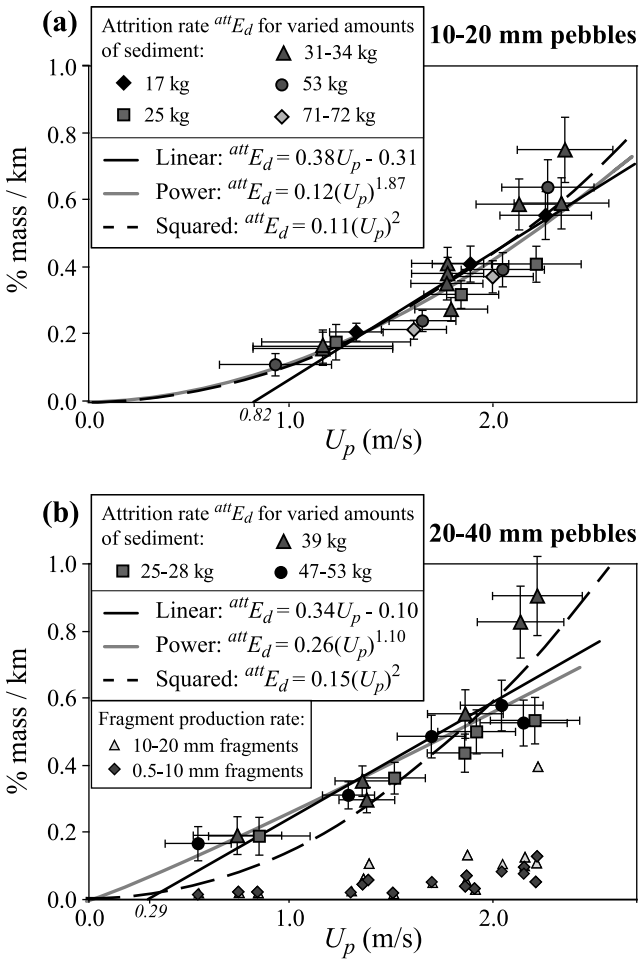

Figure 5. Attrition rate $^{att}E_d$ (in percent mass per km) as a function of pebble velocity U_p for different amounts of sediment, for experiments carried out with (a) 10–20 mm pebbles and (b) 20–40 mm pebbles. Regression curves and their equations are shown for 3 models: linear, power, and squared. In Figure 5b, the rate of fragment production $^{fr}E_d$ (in percent mass per km) is also represented.

For amounts of sediments larger than this value, pebbles are arranged in several superposed layers.

[19] The results of experiments involving varying quantities of pebbles (Set 1) illustrate how the amount of sediment controls the abrasion rates (Figure 4). To avoid the high abrasion rate variability that splitting and breaking processes can introduce (see section 3.3), only attrition rates are presented here. For the 10–20 and 20–40 mm pebbles (Figures 4a and 4b) and for a given water discharge (gray curves), an increase in the amount of sediment leads first to an increase in attrition rate $^{att}E_t$ from 0 at very low concentration to a maximum value. Then, when larger amounts of sediments are introduced, the attrition rate tends to progressively decrease, despite all the sediment being in full motion. However, the water discharge must be raised to maintain pebble velocity constant while increasing the amount of sediment. If data points are plotted with their corresponding pebble velocity instead of water discharge, the trend described by the data is noticeably different (Figures 4c and 4d). Constant–pebble velocity curves start from the origin and, after an ascending stage, reach a plateau. This plateau seems to be reached for an amount of sediment of 5–15 kg and 15–25 kg for the 10–20 and 20–40 mm fractions respectively. Here, our results suggest that the critical amount of sediment necessary to reach the plateau of Abrasion Independent of the Amount of Sediment (hereafter named "AIAS plateau") is 30 to 70% of the amount required to cover the entire flume floor with close-packed pebbles. Taking advantage of the existence of the "AIAS plateau" and considering the results obtained for quantities of pebbles larger than the critical value, we study in the following sections the dependency of abrasion rates on pebble velocity, size or lithology independently of the role of the amount of sediment. Note that in Figures 4c and 4d, and in further data analysis, we have chosen to represent the attrition rate per unit traveled distance ($^{att}E_d$) instead of attrition rate per unit time ($^{att}E_t$) because this first variable can be directly compared to downstream fining rate in natural rivers. Because ($^{att}E_d$) = ($^{att}E_t$)/U_p and because the curves of Figures 4c and 4d correspond to a constant pebble velocity, this change of variable affects neither the shape of the curves nor the previous analysis of the "AIAS plateau." However, it would have some influence on the specific definition of the rate of mass loss and on the coefficients characterizing the relationship between erosion rate and other variables such as particle size or velocity.

3.2. Pebble Velocity and Abrasion Rates

[20] The attrition rate $^{att}E_d$ (expressed in percent mass loss per unit of traveled distance) obtained for different amounts of pebbles and injection discharges increases systematically with increasing mean pebble velocity (Figures 5 and 6). In the absence of a proper physical model of pebble abrasion by interparticle collision to be tested, we consider three simple regression relationships: linear, power and squared, the later being suggested by *Kuenen*'s [1956] data. To keep the same number of free parameters, the power relationship is forced through the origin, whereas the linear model is free to vary its intercept, simulating a system with a pebble velocity threshold below which abrasion does not occur. The squared model is also forced through the origin to allow direct comparison with the power model. Data obtained using 10–20 mm pebbles (Figure 5a) offer the best opportunity to compare the models: the data set is the most complete and fragmentation, which makes the results noisier (see below), is limited. The no-threshold power model, with an exponent of 1.87, gives a better fit than the threshold linear model, with a t test value of 6.101 (statistical significance > > 99.5%). The squared model is not statistically discernable from the power model (t test value = 0.951, statistical significance < < 90%). It is worth noticing that the best fit squared relationship for this set of data passes through the origin even if it is free to vary its intercept. Results of experiments carried out with 20–40 mm pebbles display more ambiguous trends (Figure 5b): the power relationship produces the best fit with an exponent of 1.1 and is not statistically different from the linear model (t test value = 0.856, statistical significance < < 90%). The linear fit has a low velocity threshold compared to the linear model fitting the 10–20 mm pebble data. The squared model fails to accurately predict the

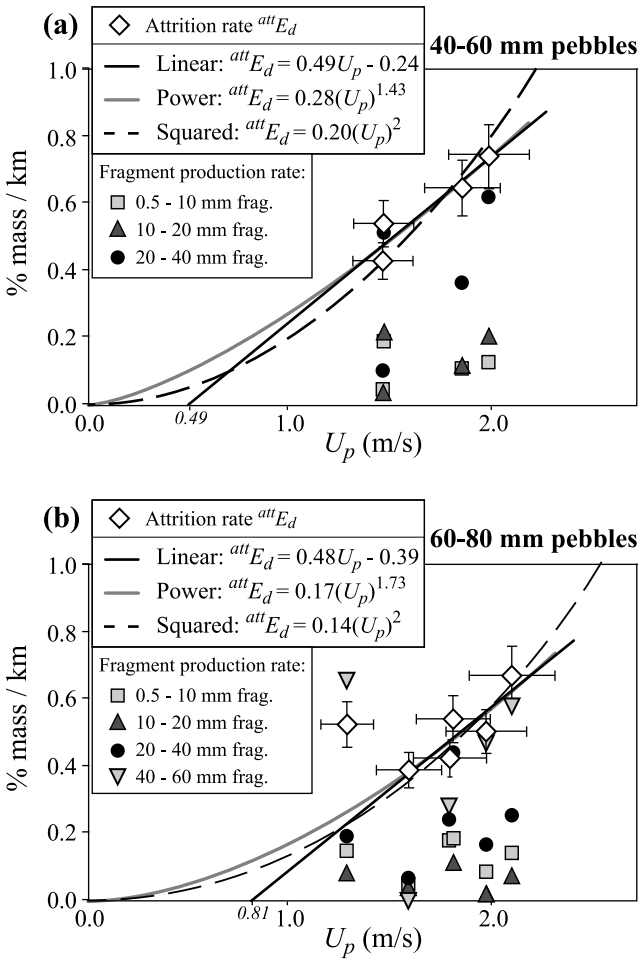

Figure 6. Rates of attrition ($^{att}E_d$) and fragment production ($^{fr}E_d$) for experiments carried out with (a) 40–60 mm pebbles and (b) 60–80 mm pebbles. The amount of sediment introduced at the beginning of the experiments ranges between 52 and 60 kg for the 40–60 mm pebbles and between 50 and 85 kg for the 60–80 mm pebbles. Regression curves and their equations for attrition data are shown for 3 models: linear, power, and squared. For clarity, error bars are drawn only for attrition data.

attrition rates at low velocities. We emphasize however that high attrition rates for $U_p < 1$ m/s could be due to impacts with immobile pebbles if the sediment is not at full motion, as discussed in section 4.1.3. Finally, the three models adequately fit the relatively small data sets obtained with 40–60 and 60–80 mm pebbles (Figure 6), if we exclude the anomalously high attrition rate obtained with 60–80 mm pebbles traveling at 1.3 m/s from the analysis. To summarize, the application of the "principle of parsimony" [*Burnham and Anderson*, 2002] would favor the squared model which contains only one free parameter and explains the data fairly well, in particular the 10–20 mm data set which is the most complete. We acknowledge however that our analysis cannot definitely rule out a linear relationship between attrition rate and mean pebble velocity, or the existence of a threshold for attrition, as suggested by the linear regressions ($^{att}E_d = 0$ for $U_p > 0$).

3.3. Products of Abrasion

[21] The attrition of 10–20 mm limestone pebbles produces more sediment in the clay- and silt-size classes than fine sand (Figure 7a), with a peak in the grain size distribution located at phi = −9 (i.e., ∼2 μm). The attrition products become more abundant when U_p increases (section 3.2) but the influence of particle velocity and size on the size distribution of these products has not been investigated. The production rate of coarser fragments by chipping, breaking and splitting also appears to increase

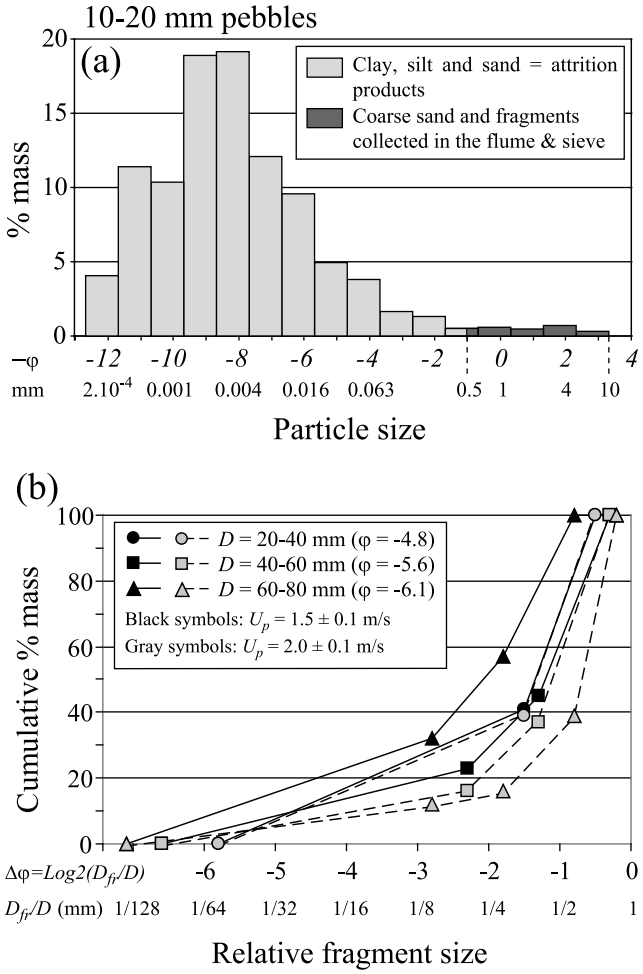

Figure 7. (a) Grain size distribution of the abrasion products collected after 18 experiments carried out with 10–20 mm pebbles. These experiments produced 19,710 g of particles finer than 0.5 mm and ∼400 g of fragments coarser than 0.5 mm, i.e., ∼2% of the total abrasion products. Grain size distribution was determined by sieving the particles coarser than 0.5 mm and using a laser grain-size analyzer for the particles finer than 0.5 mm. (b) Average grain size distributions of the fragments (>0.5 mm) produced during experiments carried out with 20–40, 40–60, and 60–80 mm pebbles (corresponding to a mean diameter D = 28, 49, and 69 mm, respectively) at mean pebble velocities U_p = 1.5 ± 0.1 m/s (black symbols) and 2.0 ± 0.1 m/s (gray symbols). D_{fr} is fragment size. The x axis is normalized fragment size: $D_{fr} - D$ in $-\varphi$ scale and D_{fr}/D in mm. The y axis is cumulative % fragment mass.

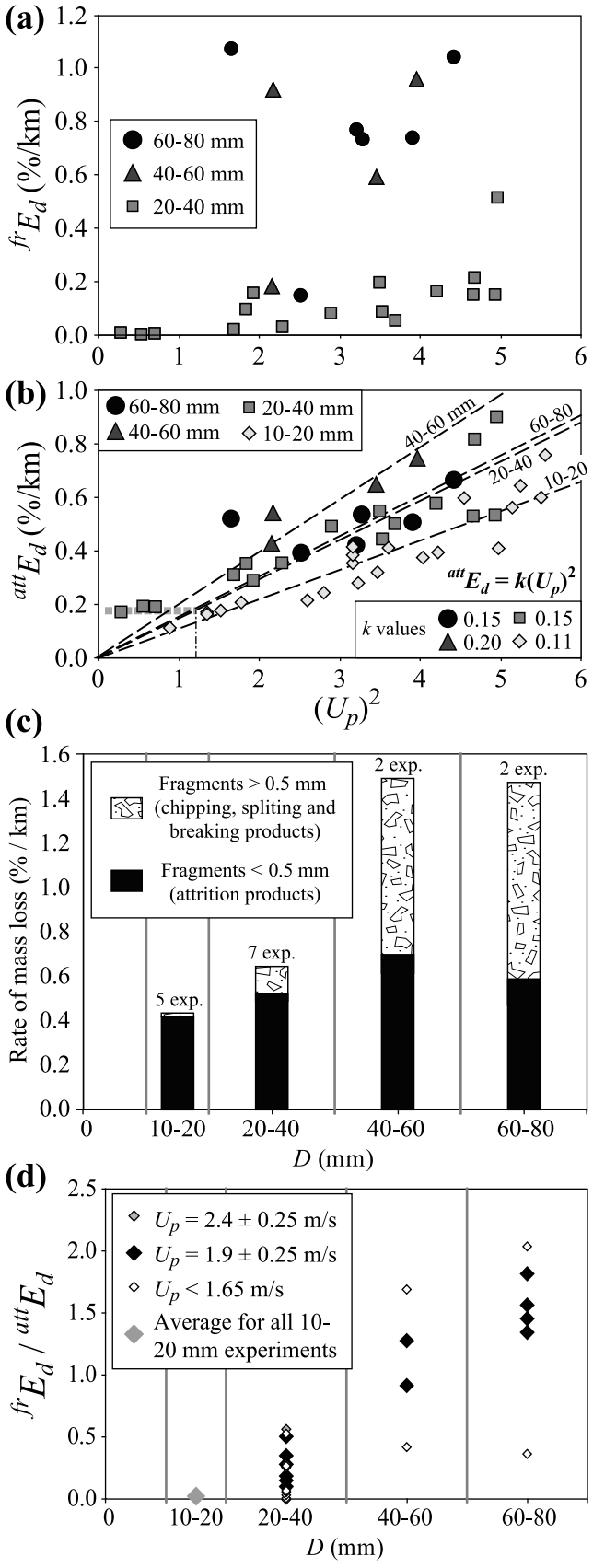

Figure 8. (a) Fragment production rate and (b) attrition rate as a function of squared pebble velocity and sediment grain size for all experiments. In Figure 8b, thick gray dotted line highlights roughly constant attrition rates at low flow stage for the 20–40 mm pebbles. (c) Average rate of mass loss by attrition and fragmentation as a function of sediment grain size for experiments carried out with a mean pebble velocity of 2.0 m/s, within error (the number of experiments included in the average is indicated on top of each column). (d) Ratio of fragment production rate $^{fr}E_d$ over attrition rate $^{att}E_d$ as a function of sediment grain size and mean particle velocity U_p for all experiments.

with increasing pebble velocity. This phenomenon is not well shown by the experiments carried out with 10–20 mm pebbles, as fragments coarser than 0.5 mm do not represent on average more than ~2% of the total mass loss (Figure 7a). On the other hand, data obtained using 20–40 mm pebbles show that, despite a significant scattering, fragment production rate $^{fr}E_d$ increases with increasing pebble velocity (Figures 5b and 8a). The scattering is amplified in the experiments performed with the large 40–60 mm and 60–80 mm pebbles (Figures 6 and 8a): despite using amounts of sediment large enough to make sure that the "AIAS plateau" was reached, abrasion rates show high variability for similar velocities. In addition, the order in which the experiments were carried out seems to influence the relative production of fragments if the same material is reused: experiments with low fragment production rates are found to systematically follow experiments carried out at high pebble velocity. As a general rule, fragments and fragmented pebbles were systematically produced by experiments for which U_p exceeded ~1.5 m/s (Figure 8a). We qualitatively observed that splitting and breaking are favored by the existence of weakness zones within the pebbles (bedding plane, schistosity, fracture, tension gash). Moreover, we observed that anomalously high attrition rates, i.e., for which the attrition rate plots above the best fit curves (Figure 6), systematically correspond to experiments characterized by high fragment production.

[22] The normalization of fragment size by the initial mean pebble size produces similar fragment size distributions for all experiments carried out with pebbles larger than 20 mm traveling at velocities in excess of 1.4 m/s (Figure 7b). For all the experiments but one, relatively large fragments are mostly produced (Figure 7b): more than 60% (in mass) of the fragments produced are larger than a third of the initial pebble size; fragments larger than a eight of the initial pebble size represent 70 to 90% of the mass of fragment produced.

3.4. Pebble Size and Abrasion Rates for Well-Sorted Material

[23] Whereas a $^{att}E_d = k(U_p)^2$ relationship can reasonably fit all our experimental data points (section 3.2), the control that the grain size exerts on the value of the coefficient k does not display obvious systematic behavior (Figures 5, 6, and 8b): the coefficient k is maximum for D = 40–60 mm but, in any case, the variation in k is modest. The average value of k is 0.17 (% mass × 10^{-3} s^2/m^3) and its standard deviation 44% when all data are included. If we exclude the four data points obtained at low pebble velocity in the 20–

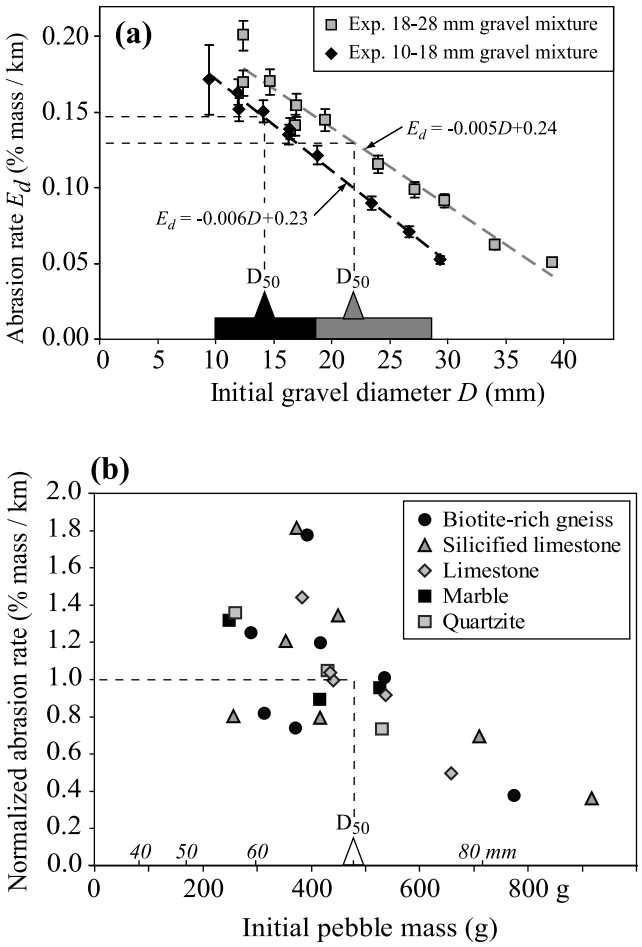

Figure 9. (a) Abrasion rates for individual limestone pebbles of different sizes eroded in the small flume with ~400 g of 18–28 mm gravel (gray squares) and 10–18 mm gravel (black diamonds). Best linear fits are displayed with equations. Boxes at the bottom of Figure 9a indicate the range of gravel size in the 18–28 mm mixture (gray box) and 10–18 mm mixture (black box). Median grain size D_{50} is shown for both mixtures by inverted triangles on boxes. (b) Normalized abrasion rates for pebbles of different lithologies abraded together in the large flume in the same experimental conditions. Abrasion rates are normalized by the average abrasion rate obtained for each lithology. For information, the equivalent grain diameter D is indicated in italic above the x axis.

40 mm and 60–80 mm data sets that depart from the parabolic relationship (Figures 5b and 6b), the average value of k is 0.15 (% mass $\times$ 10^{-3} s^2/m^3) and its standard deviation falls to 27%. The same trend is observed when attrition rate is represented as a function of pebble size for experiments conducted at similar pebble velocities (Figure 8c): maximum attrition rate is obtained for D = 40–60 mm but mass loss by attrition displays low variability despite a fivefold variation in particle diameter. Although more experiments are needed to clearly define the dependency of attrition rate on particle diameter and extend it for a larger range of particle size, our data show that this dependency is weak and that attrition rate is much more sensitive to particle velocity.

[24] In contrast to attrition, fragment production strongly depends on particle size: pebbles with $D \geq 40$ mm exhibit fragment production rates (Figures 8a and 8c) and fragment-production-rate-to-attrition-rate ratios (Figure 8d) which are much higher than those obtained with smaller pebbles. Pebble size exerts in that sense an unambiguous control on the total abrasion rate by abruptly enhancing the production of fragments for pebbles larger than 40 mm (Figures 8a, 8c, and 8d).

3.5. Pebble Size and Abrasion Rates for Poorly Sorted Material

[25] When poorly sorted material which mimics an alluvium with a realistic grain size distribution is used, the circular flume tends to produce a radial segregation of sizes. To partly avoid this problem, single pebbles of different sizes were diluted in well-sorted material (Set 3). The effect of the difference between a pebble grain size and the material median grain size on pebble abrasion rate was then investigated. To reduce dispersion due to breaking processes and to lithologic differences between pebbles, the experiments were carried out in the small flume where attrition is the dominant process, and with artificially made pebbles from a single homogeneous piece of limestone. Two granitic pebble mixtures with different median grain sizes were used (Figure 9a): 10–18 mm with D_{50} = 14 mm and 18–28 mm with D_{50} = 22 mm. Individual limestone pebbles with sizes in the ranges 9–29 mm and 12–39 mm were introduced into the 10–18 mm and 18–28 mm mixtures respectively. Despite the threefold variation in individual pebble size, pebble velocities were found to be relatively homogeneous: average velocity was 0.64 m/s for the 9–29 mm pebbles in the 10–18 mm mixture, with a standard deviation of 3%; average velocity was 0.75 m/s for the 12–39 mm pebbles in the 18–28 mm mixture, with a standard deviation of 7%.

[26] There is a systematic decrease in abrasion rate with increasing initial pebble diameter D (Figure 9a). This trend, which appears linear in the investigated range of pebble size, is observed for the two pebble mixtures. A similar but less systematic trend is observed with pebbles of different size and lithologies that were used to investigate the abrasion dependence on lithology (section 3.7). Experiments (Set 2) were carried out in the large flume with pebbles from varied lithology, the size of which ranged between 40 and 80 mm (Figure 9b). Despite larger dispersion due to the heterogeneity of the natural pebbles sampled on gravel bars and to the fragmentation processes which are more effective in the large flume, the global trend observed for almost all lithologies is a decrease in abrasion rate with increasing pebble size, as observed in Set 3. A similar behavior had been previously observed by *Kodama* [1994b]: in his experiments (see Kodama's Figure 11), the abrasion rate of large pebbles was reduced when pebbles were mixed with poorly sorted material instead of well-sorted material; the opposite trend was observed for small pebbles (see Kodama's Figure 11), whatever attrition or breaking was the dominant process.

3.6. Influence of Bed Condition

[27] In natural rivers, moving pebbles lose mass when they impact other moving pebbles, but they also experience substantial abrasion when they hit either bedrock or immobile

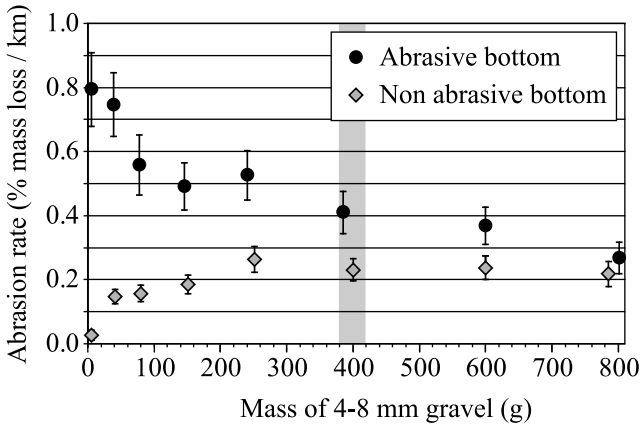

Figure 10. Abrasion rate as a function of sediment amount for two different floor conditions (experiments were carried out with 4–8 mm limestone gravel in the small flume). First subset of experiments (4a, diamonds) was carried out with a rubber floor. Second subset (4b, circles) was conducted with a floor covered with one glued layer of close-packed gravel with the same size and lithology as the gravel transported in the flume. Vertical shaded area corresponds to the approximate amount of sediment for which the flume floor is fully covered with pebbles.

pebbles. The nonabrasive bed condition in previous experiments was imposed in order to suppress the latter component of the abrasion and isolate a single process. However, before any transposition of our experimental results to abrasion in natural rivers, it is important to quantify the contribution of the impacts with the floor. We therefore glued limestone gravel (4–8 mm) to a removable floor and carried out experiments in the small flume with different amounts of gravel of the same size and from the same origin (Set 4). Two subsets of experiments were carried out with two distinct floors of equivalent roughness: a nonabrasive rubber floor and an abrasive pebbly floor (subsets 4a and 4b respectively). For a given amount of gravel, the difference in mean pebble velocity induced by the change in bed condition is on average 5% and does not exceed 10%. For the first subset (4a), as is already observed in the large flume (section 3.1), abrasion rate first increases with increasing amount of sediment (Figure 10). Abrasion rate then reaches an asymptotic value close to 0.25%/km for an amount of sediment roughly equivalent to half the amount required to cover the floor of the flume with close-packed pebbles ($M_{sc} \approx 410$ g for 4–8 mm gravel in the small flume, see section 3.1). This subset of the experiments thus confirms the existence of the AIAS plateau (section 3.1 and Figures 4c and 4d). The second subset of experiments (4b) shows an inverted trend (Figure 10): for reduced amount of sediment, most of the impacts are occurring with fixed pebbles on the floor and these collisions promote much higher abrasion rates (3.5 times higher) than the rates associated with impacts between moving gravel when the AIAS plateau is reached. However, when the amount of sediment increases, the contribution of the impacts with the floor decreases first rapidly (for amounts up to half the amount required for covering the floor with close-packed pebbles) and then more gently, leading to a progressive convergence between the curves of subsets 4a and 4b. When the amount of sediment reaches 800 g, i.e., when the sediment amount is equivalent to two layers of close-packed gravel, the abrasion rate is close to the value of 0.25%/km obtained with the nonabrasive floor. For such an amount of sediment, collisions between moving particles thus largely predominate over collisions with the floor.

3.7. Pebble Lithology and Abrasion Rates

[28] To explore the lithologic control on abrasion rates, two experiments were carried out with 15 kg of 40–80 mm pebbles of various lithologies mixed with 60 kg of 40–80 mm pebbles of Alpine igneous crystalline rocks [*Attal and Lavé*, 2006] (Set 2). Hydrodynamic conditions were chosen to be of the same order as those prevailing during the annual peak discharge in large mountain rivers. Injection discharge was set to 97 l/s, which in that case corresponds to a mean flow velocity of 2.3 m/s, a mean pebble velocity of 1.2 m/s for this grain size, and an average basal shear stress of $\sim$250 N.m^{-2}. The total sediment amount of 75 kg ensured that the "AIAS plateau" was reached.

[29] As evidenced by previous experimental studies [e.g., *Schoklitsch*, 1933; *Kuenen*, 1956; *Bradley*, 1970; *Kodama*, 1994b; *Lewin and Brewer*, 2002], lithology exerts a very important control on pebble abrasion rate (Figure 11). The abrasion rate is 500 times higher for unconsolidated sandstone (up to 50%/km) than for the strongest quartzite (0.1%/km). Soft lithologies (schist and sandstone) present in general a much more important dispersion in abrasion rates than resistant lithologies (quartzite and granite) or moderately resistant lithologies (gneiss, limestone and marble). For these soft lithologies, our experimental abrasion rates are 4 to 20 times higher than previously published rates. In contrast, our abrasion rates were found to be only 1 to 3 times larger than previous estimates for resistant lithologies (Figures 11a and 11b), if we except the highly vigorous experiments carried out in a tumbling barrel by *Kodama* [1994b] (Figure 11b).

[30] Detailed observation of the pebbles of various lithologies used in our experiments brings additional insights into the factors that control rock resistance to abrasion. The nature and strength of the constitutive minerals exerts a primary control on pebble abrasion rates: calcite-bearing rocks (limestone, marble) are less resistant than quartz-bearing rocks (quartzite, granite, gneiss), while silicification of limestone greatly enhances its resistance to abrasion (Figure 11a). Low-strength phyllitic minerals weaken the rocks: schists which are rich in phyllitic minerals are quickly abraded. Biotite-rich and aluminous gneisses exhibit higher abrasion rates than calcic gneisses which contain less phyllitic minerals. In addition, phyllitic minerals present a strong mechanical anisotropy: when they are preferentially oriented within foliated rocks, the resistance to abrasion is further lowered, as observed for gneisses that are abraded faster than isotropic but mica-rich granites. Cohesion between minerals also plays an important role in controlling pebble abrasion rates. Sandstone diagenesis results in grain cementation and rock porosity reduction. This phenomenon increases rock resistance to abrasion: weakly cemented sandstones are abraded much faster than cemented ones. Finally, joints (including bedding planes, schistosity, fractures and tension gashes) constitute

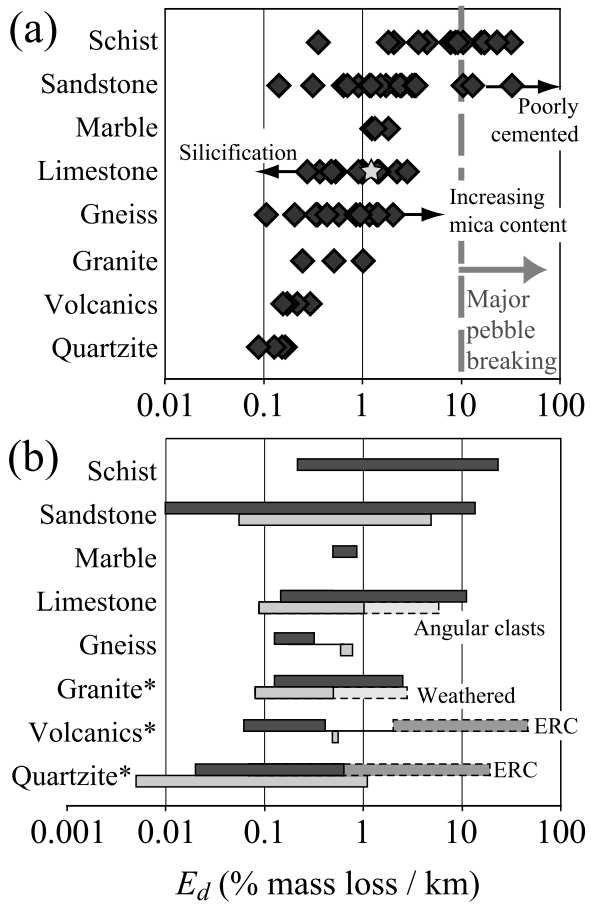

Figure 11. Influence of lithology on abrasion rates. (a) Summary of our experiments carried out with 15 kg of pebbles of different lithologies mixed with 60 kg of 40–80 mm igneous crystalline pebbles; water discharge was 97 l/s [*Attal and Lavé*, 2006]. Star represents mean abrasion rate for 5 Buech limestone pebbles that were included in this set of experiments. (b) Compilation of previously published experimental abrasion rates for similar groups of lithologies [*Schoklitsch*, 1933; *Bullows*, 1939; *Krumbein*, 1941; *Kuenen*, 1956; *Bradley*, 1970; *Adams*, 1978; *Mikos*, 1994; *Kodama*, 1994b; *Jones and Humphrey*, 1997; *Lewin and Brewer*, 2002]. Size and mass diminution coefficients have been converted to abrasion rates (in % mass loss/km). Light gray boxes are flume data, and dark gray boxes are tumbling barrel data. Light-colored dashed boxes correspond to data obtained in experiments carried out with angular clasts, with weathered clasts or in *Kodama*'s [1994b] vigorous ERC tumbling barrel (with impact velocities up to 2 m/s). Asterisks: "Granite" and "Volcanics" include different types of intrusive and extrusive igneous rocks, respectively; "Quartzite" includes different types of siliceous rocks: quartzite, flint, chert, agate, radiolarite, and obsidian.

weakness zones which can favor abrasion (section 3.3). In schists and mica schists, the combination of schistosity planes and high content of phyllitic minerals promotes high abrasion rates and pebble splitting. The important point is that lithology controls not only abrasion rates but also abrasion processes [see also *Kodama*, 1994b].

[31] Pebble abrasion rates are also expected to depend on the lithology of the pebbles with which they are mixed. Five pebbles of the fine-grained limestone which has been used in the Set 1 experiments were introduced in the multi-lithology Set 2 experiments. Mixed with a majority of igneous pebbles, the limestone pebbles were abraded at a rate of 1.15 ± 0.4%/km, i.e., 2 to 3 times faster than if they had been mixed with other limestone pebbles in the same conditions (for similar amount of sediment, grain size and particle velocity, ${}^{att}E_d \sim 0.3–0.4$%/km and $E_d \sim 0.5$%/km). Impacts with more resistant lithologies therefore significantly enhance abrasion efficiency. *Sklar and Dietrich* [2001] similarly documented a threefold increase in their experimental bedrock abrasion rates when limestone bedrock was abraded by quartzite pebbles rather than by limestone pebbles. The experimental pebble abrasion rates presented in Figure 11a have therefore to be considered within the framework of our experiments, i.e., valid for pebbles mixed with resistant igneous rocks. However, because resistant pebbles are predominant in mountain rivers [e.g., *Attal and Lavé*, 2006], we believe that our experimental abrasion rates would be valid in many natural settings.

4. Discussion

4.1. Sensitivity of Abrasion Rates and Processes to the Controlling Variables

4.1.1. Products of Abrasion

[32] Observations with the high speed camera suggest that collision is the dominant type of contact between particles during our experiments. We therefore infer that most of the abrasion results from dynamic impacts between particles with nonnegligible relative velocities. These dynamic contacts produce two populations of abrasion products for our limestone pebbles (section 3.3): large fragments and very small ones, with a gap in the 0.5–10 mm fraction (Figures 5b, 6, and 7). Such gap justifies a posteriori our choice of a cutoff at 0.5 mm to separate the products of fragmentation and attrition, that might relate to two distinct brittle deformation processes: the activation of large planes of rupture at the scale of the pebble (leading to the detachment of large fragments) and the coalescence of microfractures at the scale of the contact zone, respectively. Abrasion by attrition is dominant at low velocity and for small particles (<40 mm in the case of limestone), whereas fragmentation becomes dominant for large pebbles transported at high velocity (section 3.3, 3.4 and Figure 8). However, experiments involving varied pebble sizes and velocities produced similar normalized fragment size distributions (Figure 7b), suggesting that the mechanics of the fragmentation process are relatively independent of these two variables.

[33] If the influence of the controlling factors on attrition rate can be investigated and discussed in the following, the influence of these factors on the rate of fragment production is however difficult to establish because fragment production shows high variability in our experiments (Figure 8a). Because of the stochastic behavior of the chipping, breaking and splitting processes, more experiments would be required to produce meaningful trends. In addition, our results are probably biased by the use of the same pebbles

for successive experiments, since fragmentation depends on the initial state of the pebbles. For example, experiments with low fragment production rates are found to systematically follow experiments carried out at high velocity (section 3.3): if splitting is favored by high energy impacts, the number of weakness zones in pebbles might dramatically decrease during high velocity experiments, possibly reducing the effectiveness of the splitting and breaking processes in the following experiment conducted at lower pebble velocity.

[34] Finally, it has to be noted that our results are valid for rounded particles. The abrasion rate of angular clasts has been found to be up to 5 times higher than the abrasion rate of similar rounded pebbles, due to the preferential abrasion of corners and edges, mostly by chipping [*Kuenen*, 1956; *Lewin and Brewer*, 2002]. However, it has been shown that the rounding of corners and edges is rapid and that such high abrasion rates due to the high angularity of clasts are limited to the first few kilometers of transport along rivers [e.g., *Krumbein*, 1941; *Kuenen*, 1956]. For that reason, and despite most particles delivered by hillslopes to the fluvial network being angular, we will neglect in the following this phenomenon affecting pebbles as they begin their journey along the river.

4.1.2. Influence of Lithology on Abrasion Rates and Processes

[35] As already emphasized in previous studies, lithology exerts the most important control on pebble abrasion rates and processes [*Schoklitsch*, 1933; *Kuenen*, 1956; *Bradley*, 1970; *Kodama*, 1994b; *Lewin and Brewer*, 2002]: the weakest lithology tested in our experiments is abraded 500 times faster than the strongest one (section 3.7). We also observe that fragment production rate is highly lithology dependent [*Kodama*, 1994b]: fragmentation is limited in resistant and compact lithologies but is the dominant abrasion process in jointed rocks. Because our experimental flume reproduces breaking and chipping processes at high impact velocities more efficiently than the tumbling barrels which were often used in previous studies, our experimental abrasion rates are consistent with or slightly higher than previously published abrasion rates for resistant and compact lithologies (e.g., quartzite, granite, limestone) but are up to an order of magnitude higher than published abrasion rates for weak or jointed rocks (mostly sandstone and schist; Figures 11a and 11b). Future steps in this research will involve linking these variations in attrition and fragmentation production rates to the mechanical properties of the rocks, such as tensile strength [*Sklar and Dietrich*, 2001] or joint spacing.

4.1.3. Amount of Sediment, Pebble Velocity, Bed Condition, and Transport Stage

[36] The existence of the AIAS plateau suggests that the frequency of collision between moving pebbles increases continuously with increasing amount of sediment until reaching a plateau for around half the amount of sediment necessary to cover the flume floor with close-packed pebbles (Figures 4 and 10). Therefore, if the sediment is not at full motion and the amount of sediment in motion is lower than this critical amount, collisions with resting pebbles can no longer be neglected. In our experiments, it was observed on the high-speed camera movies that full motion of one layer of pebbles occurs at mean pebble velocities of ~1.5, ~1.2 and ~1.0 m/s for the 60–80 mm, 20–40 mm, and 10–20 mm pebbles respectively. For the 20–40 mm pebbles, we indeed observe that below this critical velocity ($U_p \leq 1.2$ m/s), attrition rates are higher than what the regression relationships would predict, in particular the relation ${}^{att}E_d = k(U_p)^2$ which fits the data fairly well (section 3.2 and Figures 5 and 8). This is what would be expected if a large proportion of the moving pebbles were impacting immobile particles. Below this threshold, attrition rate seems to become roughly constant (Figures 5 and 8b). We thus hypothesize that pebble attrition rate in channel beds made of loose sediments is proportional to $(U_p)^2$ at transport stages above full motion of a gravel layer but becomes approximately constant at low flow stage, due to infrequent pebble motions and high mass loss when moving pebbles impact immobile pebbles. Future additional experiments near incipient pebble motion, using a modified flume to reduce the large radial velocity gradient observed at low pump discharge (e.g., including additional flow injections along the internal wall of the flume [*Lewin and Brewer*, 2002]) are however required to better document such a trend.

[37] In our experiments, we analyzed independently the influence of the amount of sediment, pebble size, pebble velocity and bed condition on pebble abrasion rates. In natural rivers, these variables are intimately linked: they depend on the transport stage, i.e., the ratio τ^*/τ^*_c, where τ^* and τ^*_c are the dimensionless Shields stress and critical Shields stress for particle entrainment, respectively. For saltating particles, mean hop velocity appears to depend on τ^*/τ^*_c and on the grain size D, according to the following relation [*Sklar and Dietrich*, 2004]:

$$u_p \propto \sqrt{\frac{\rho_s - \rho_w}{\rho_w}}\sqrt{D}\left(\frac{\tau^*}{\tau^*_c} - 1\right)^{0.5}, \tag{5}$$

where ρ_s and ρ_w are the density of the sediment and water respectively. According to our experimental results (Sets 1 and 4), at high flow stage, i.e., at full pebble motion, most collisions occur between moving pebbles and $U_p \approx u_p$. On the basis of the apparent relation between attrition rate and $(U_p)^2$, we propose that

$${}^{att}E_d \propto D(\tau^*/\tau^*_c - 1) \tag{6}$$

at full motion (Figure 12). For lower values of transport stage, as stated above from a reduced set of experiments with 20–40 mm pebbles, we hypothesize that attrition rate increasingly departs from the linear trend in equation (6) when approaching incipient pebble motion ($\tau^*/\tau^*_c = 1$) and would tend to be roughly constant at low transport stage due to dominant impacts with immobile pebbles and increased number of impacts per unit length (Figure 12). In our experiments, it was found that incipient full motion of one layer, i.e., the threshold between the constant and linear domains in Figure 12, occurs at transport stage of $\tau^*/\tau^*_c \approx 3.3 \pm 0.3$, independently of the grain size.

4.1.4. Influence of Pebble Size on Abrasion Rates and Processes

[38] In our experiments, pebble size was found to be the least determinant parameter on pebble attrition rate when well sorted material was used (section 3.4). However,

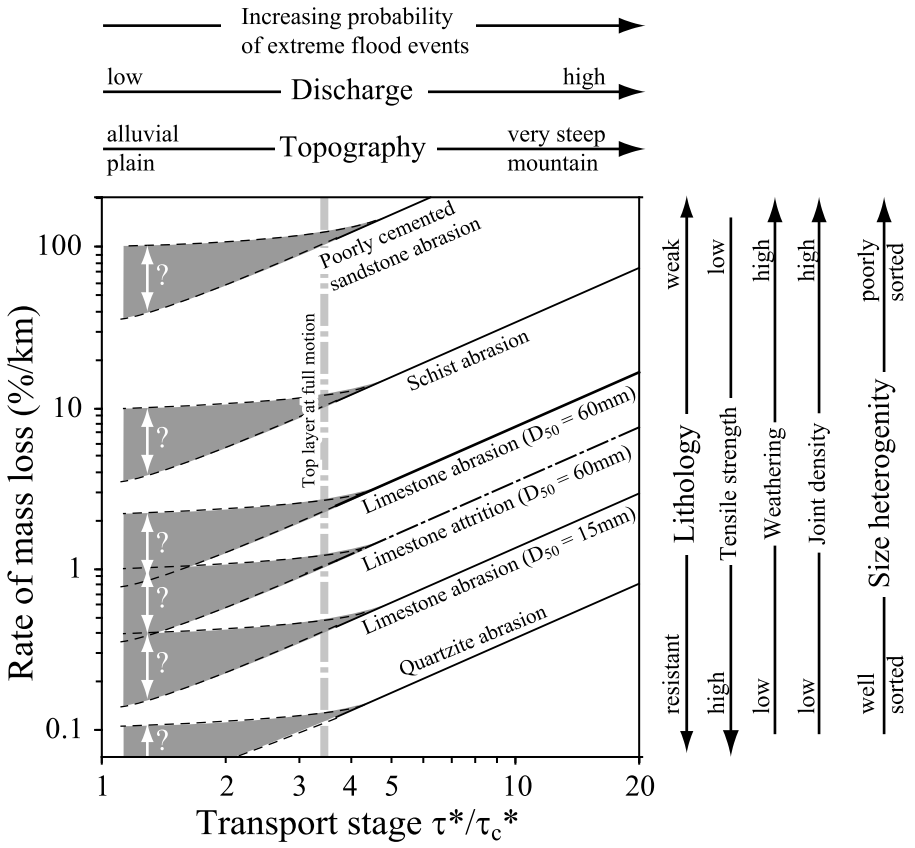

Figure 12. Semischematic diagram of the abrasion rate dependency on transport stage. The curves are drawn according to the experimental results of Set 1 and equation (6). For simplicity, total abrasion rate, i.e., including fragmentation, is assumed to scale linearly with transport stage, as does the attrition rate. It is also assumed that 60 mm pebbles in other lithologies present the same dependency on transport stage as limestone pebbles; the positioning of the curves was done according to the results of the Set 2 experiments (Figure 11) during which transport stage was ~3.5. Shaded areas at low transport stage ($\leq$3.3) represent possible data domain, with abrasion rates higher than predicted by the linear trend due to impacts with immobile particles. Note that abrasion rate values are given for pebbles mixed with resistant particles (e.g., igneous rock) and in the case of well-sorted material. Having poorly sorted material with large differences in pebble mobility and velocity would move the curves upwards.

particle velocity depends on particle size: according to equation (6), attrition rate is expected to increase linearly with particle size at a given transport stage (Figure 12). Our experiments also showed that fragment production is favored by impacts involving large particles with, in the case of our limestone pebbles, a sharp increase in fragment production rate above $D \sim 40$ mm (Figures 8c and 8d). For fractured, jointed or schistose lithologies, abrasion rate is therefore expected to largely increase with pebble size, as well as with pebble velocity and transport stage. Finally, bed load material in natural rivers is rarely well sorted. The results of our Set 3 experiments (section 3.5) show that the attrition rate of a given pebble depends on its size relative to the median size of the pebble mixture (Figure 9): the larger the particle, the lower the particle abrasion rate. This phenomenon might result from the fact that two particles with the same characteristics except mass should experience similar mass losses when they collide; as the mass loss is divided by the particle mass to calculate the abrasion rate, a higher abrasion rate is thus obtained for the smallest particle. In natural settings, poorly sorted material may include a much larger range of particle sizes than in our experiments and may thus promote significant differences in particle mobility, with the largest particles potentially remaining motionless. Such differences in mobility would favor larger relative impact velocities between particles and increase abrasion efficiency: our experimental abrasion rates are therefore probably minimum estimates of natural rates at low and medium transport stages.

4.2. Abrasion and Fining Coefficients in Natural Rivers

4.2.1. Evolution of Particle Size Along Fluvial Networks in Varied Geomorphic Settings

[39] When using the Sternberg exponential equation (equation (1)) to compare the fining coefficient to pebble abrasion rate, it is implicitly assumed that the abrasion rate of a specific lithology is constant along a river. According to our results, abrasion rate is constant as long as the pebble velocity is held constant and the fragmentation process is ineffective (the abrasion rate of a particle would otherwise decrease downstream as the particle is progressively reduced in size).

[40] The abrasion rate of a pebble is primarily controlled by the transport stage (Figure 12). In a given morphostructural

setting (e.g., sedimentary basin, mountainous area), the river concavity index θ which is the exponent in the relationship $S \propto A^{-\theta}$ (where S is river slope and A is drainage area) is generally invariable. In mountainous areas, θ is typically close to 0.5 [e.g., *Sklar and Dietrich*, 1998]. Assuming that river geometry obeys typical hydraulic scaling laws, i.e., channel width scales with the square root of drainage area [e.g., *Leopold and Maddock*, 1953; *Montgomery and Gran*, 2001] and width-to-depth ratio is approximately constant along the river [e.g., *Leopold and Maddock*, 1953; *Finnegan et al.*, 2005], it can be shown that fluvial shear stress and thus mean pebble velocity are roughly constant along the river (note that these two assumptions have been shown to not apply in various mountainous settings, in particular in transient landscapes [e.g., *Whittaker et al.*, 2007]). On the basis of the assumptions above, abrasion rate can thus be considered constant in first approximation in a given morphostructural setting, except for lithologies prone to breaking in highly dynamic environments: in such a case, a sharp decrease in abrasion rate would be expected when a particle's size is reduced below the size over which fragmentation is dominant (section 4.1.4). However, abrasion rate is expected to vary according to the setting: for example, the abrasion rate of a pebble which traveled in a steep mountain river probably decreased significantly when the pebble arrived in a foreland basin characterized by much lower transport stages.

[41] In alluvial plain settings, rivers are characterized by shallow slopes and the transport stage during sediment transport and channel form adjustment is believed to be close to 1.5 [e.g., *Ikeda et al.*, 1988]. In such rivers, the opposing effects of low pebble velocity and dominant impacts between moving particles and immobile ones are expected to produce abrasion rates higher than the relation ${}^{att}E_d = k(U_p)^2$ would predict (Figure 12). However, because of the low particle velocity, pebbles would be reduced mostly by attrition rather than by fragmentation.

[42] In contrast, abrasion rates are maximized in rivers flowing across active mountains like the Central Range of Taiwan or the Himalayas, particularly if pebble lithologies are prone to breaking and splitting. In such rivers characterized by steep slopes, high pebble velocities would promote high rates of attrition and fragment production [e.g., *Attal and Lavé*, 2006]. In the case of our 40–80 mm limestone pebbles, attrition and abrasion rates could be as high as 4%/km and 10%/km respectively at transport stage of ~10–15 (Figure 12). These rates are minimum estimates, given that high fragment production rates would in turn enhance all pebble abrasion processes since angular fragments can be up to five times more erodible than rounded fragments [*Kuenen*, 1956]. In addition, the range of grain sizes in such rivers is usually wide and includes boulders that remain motionless during most of the floods. In this case, impacts between moving pebbles and immobile boulders would lead to high abrasion rates, as emphasized by the results of the subset 4b experiments with low amount of sediment and pebbles glued on the floor of the flume (section 3.6 and Figure 10).

[43] Finally, it is to be noted that, because pebble abrasion rate depends on the transport stage, it will vary with flood intensity (Figure 12). Estimating pebble abrasion rate during fluvial transport therefore requires averaging its value over the whole flood distribution. Abrasion rate will depend on climate regime in a nonlinear fashion, where the precise relation is determined by the interplay of the threshold discharge for sediment transport and the magnitude-frequency distribution of floods.

4.2.2. Evolution of Sediment Load Characteristics Along Fluvial Networks and Implications for Downstream Fining in Natural Rivers

[44] Along natural streams, several studies have focused on sediment transport and dispersion using tracers [e.g., *Ferguson et al.*, 1996]. But, to our knowledge, none has focused on the abrasion of these pebbles during their transport. In fact, most studies on abrasion along natural rivers rely on the downstream evolution of the median grain size in surface or subsurface of exposed gravel bars. However, is a direct comparison of experimental abrasion rates and downstream fining coefficients pertinent?

[45] A few authors have emphasized that abrasion rates and fining coefficients can be directly compared only when the sediment source is a point source localized in the headwater of a catchment [e.g., *Bradley*, 1970; *Ferguson et al.*, 1996; *Heller et al.*, 2001]. In that case, the spatial fining along the river will reflect the fining by abrasion of each pebble during its journey along the river. If there is no significant downstream variation in flow stage or in the fragmentation-to-attrition ratio, these regional fining ratios will follow Sternberg's exponential relation (equation (1)), with the fining coefficient δ being equal to $E_d/3$ (see equation (3)). It has to be noted, however, that such an end-member requires specific conditions, in particular a long river reach without active erosion or deposition (neutral bypass). This is probably the case of the Red Deer River (Alberta) [*Shaw and Kellerhals*, 1982] which originates in the Canadian Rocky mountains and then drains through a plain in which it is incised by 20 to 100 m. This embankment situation prevents major deposition or lateral input of coarse sediment. The median grain size of the sediment is similar to those used in our experiments (10 to 60 mm) [*Shaw and Kellerhals*, 1982] and the transport stage is ~2 at Red Deer for the 100 year flood (Q = 1900 m3/s) [*Alberta Infrastructure and Transportation*, 2007]. The fining rate values of δ = 0.1 to 0.2%/km measured along the river [*Shaw and Kellerhals*, 1982] are consistent with our experimental size reduction rates ($=E_d/3$) of the dominant lithologies, i.e., 0.03–0.07, ~0.1–0.2 and ~0.2–0.4%/km for quartzite, granite and limestone pebbles respectively (Figures 11 and 12).

[46] However, in many alluvial settings, streams drain aggradational areas: efficient selective sorting can take place there [*Brierley and Hickin*, 1985; *Brewer and Lewin*, 1993; *Ferguson et al.*, 1996; *Surian*, 2002; *Constantine et al.*, 2003] and the fining trend will no longer reflect abrasion processes alone. In such aggrading settings, size reduction rates frequently exceed 3%/km (which corresponds to a size reduction by a factor of ~2 after 20 km) [e.g., *Surian*, 2002] and abrasion would therefore be responsible for a significant part of the downstream fining only along rivers draining lithologies with abrasion rates in excess of 9%/km: such rates correspond to poorly resistant lithologies like poorly cemented sandstone, easily fragmented schists (Figure 12) or weathered pebbles in low gradient rivers characterized by

long periods of sediment storage [*Bradley*, 1970; *Jones and Humphrey*, 1997].

[47] Conversely, if there is any significant sediment input along the stream, addition of fresh material will also alter the fining trend [*Knighton*, 1982; *Parker*, 1991; *Heller et al.*, 2001; *Attal and Lavé*, 2006; *Sklar et al.*, 2006]. *Attal and Lavé* [2006] showed for example that in the case of a monolithologic watershed with hillslopes delivering to the fluvial network a unique grain size D_0 at a constant rate, the bed load flux and the fining ratio will both converge asymptotically downstream toward constant values. This asymptotic behavior results from the balance between the quantity lost by abrasion and the continuous supply of fresh material from the hillslopes (note, however, that the products of abrasion are presumed to be transported as suspended load in this model). These asymptotes depend on the fluvial network geometry: if the drainage area increases linearly with distance along the river (i.e., Hack's exponent = 1 [*Hack*, 1957]), the fining ratio first roughly follows a Sternberg-like exponential with an exponent $\delta = E_d/6$ before reaching a value of 3/4 after a distance of $\sim 250/E_d$ [*Attal and Lavé*, 2006]. Bed load flux also reaches an asymptote after a similar distance. Meanwhile the fraction of the load remaining in the bed load (which would be equivalent to the bed-load-to-total-load ratio if there were no deposition along the river) tends toward 0. In most natural fluvial networks however, the Hack's exponent ranges between 0.5 and 0.6 [*Hack*, 1957]. For a value of the Hack's exponent of 0.5, it can be shown (see Appendix A for derivation) that the fining ratio also first follows a Sternberg-like exponential but with an exponent $\delta = 2E_d/9$, and then converges toward a value of 9/16 after a distance of $\sim 400/E_d$ (Appendix A and Figure 13a).

[48] If contrasted lithologies are exposed in the catchment, we have to consider the evolution of a sediment load made of a mixture of several lithologies with distinct erodibility. In the following, we use *Attal and Lavé*'s [2006] model of sediment evolution (Appendix A) and consider a catchment characterized by a Hack's exponent of 0.5 in which sediment supply to the river is a mixture including various proportions of 3 contrasted lithologies: a resistant one (E_d = 0.2%/km, e.g., quartzite, granite), a moderately resistant one (E_d = 2%/km, e.g., limestone) and a poorly resistant one (E_d = 20%/km, e.g., poorly cemented sandstone, schist). Mixture 1 represents a sediment supply containing equal amounts of each lithology.

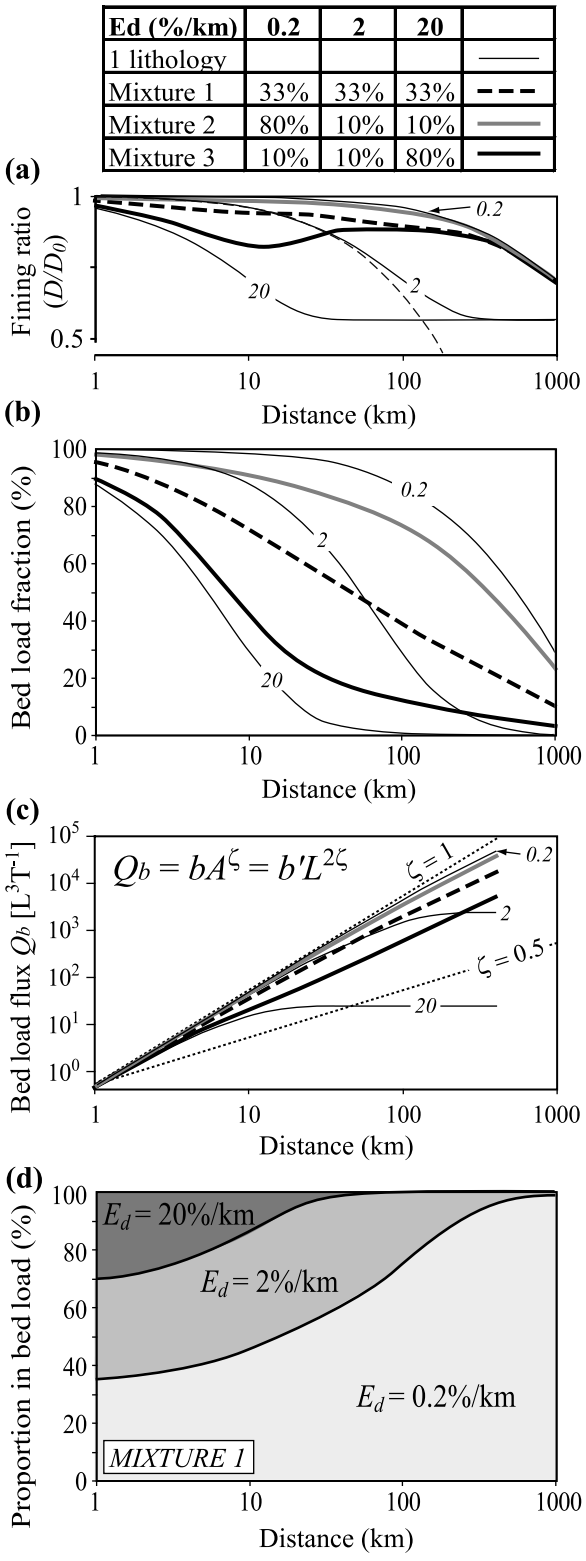

Figure 13. Downstream evolution of sediment characteristics predicted by a simple model of sediment erosion and transport derived from *Attal and Lavé* [2006] (see text and Appendix A). In the model, the products of abrasion are transported as suspended load. Key is at the top of the plots. (a) Bed load fining ratio; (b) fraction of the sediment supplied remaining in bed load; and (c) bed load flux for a sediment load composed of only one lithology (thin solid lines with abrasion rate E_d indicated on the curves) and for 3 mixtures composed of varied amount of a resistant, a moderately resistant, and a poorly resistant lithology. In Figure 13a, thin dash line represents $D/D_0 = e^{-(2Ed/9)*L}$ with E_d = 0.02 km^{-1}. In Figure 13c, we assume that 1 unit drainage area supplies 1 unit bed load (dimension [L^3]) per unit time. A power relationship is found for the 3 mixtures and when only one resistant lithology is considered: $Q_b = bA^{\zeta}$, where b and ζ are constants. Values of ζ are 0.74, 0.85, 0.93, and 0.95 for Mixtures 3, 1, and 2 and in the only one resistant lithology case, respectively. Curves corresponding to $\zeta = 0.5$ and $\zeta = 1$ are drawn (dotted lines). (d) Evolution of the proportion of the 3 lithologies for Mixture 1.

Mixture 2 is composed mostly of the most resistant rock type (80%), simulating the supply of sediment to a river draining the core of a mature mountain belt. Mixture 3 is composed mostly of the least resistant rock type (80%) and could represent the sediment supply to a river incising into a young mountain range, the sedimentary cover of which has not yet been stripped away. The fraction of the sediment supplied to the river remaining in the bed load significantly differs for the 3 mixtures and is mostly influenced by the most abundant lithology (Figure 13b). This contrasts with the behavior of the bed load fining ratio (Figure 13a): for all the mixtures, the strongest lithology controls the evolution of the grain size of the bed load. After an initial decrease, the fining ratio for all the mixtures converges toward the curve corresponding to the monolithologic experiment with the strongest lithology.

[49] The above models depicting a mountain setting in which sediment supply to the river is uniform clearly indicate that the downstream evolution of the fining ratio does not directly represent in such setting the pebble size reduction rate by abrasion (E_d/3): in the most favorable case of a monolithologic catchment and for $L \leq 300/E_d$, the fining coefficient represents 1/2 (Hack's exponent of 1 [*Attal and Lavé*, 2006]) to 2/3 (Hack's exponent of 0.5) of the pebble size reduction rate. In addition, the maximum range of size reduction is expected to fall between 25% (Hack's exponent of 1 [*Attal and Lavé*, 2006]) and 40% (Hack's exponent of 0.5; Figure 13a), which makes such fining difficult to observe due to generally large dispersion of pebble size values on gravel bars [e.g., *Attal and Lavé*, 2006]. In most cases, i.e., at distances beyond the convergence onto an asymptote or for mixtures of contrasted lithologies (Figure 13a), the fining curve no longer corresponds to an exponential but rather reaches a roughly uniform value, as confirmed by field studies in this type of setting with continuous lateral sediment supply [e.g., *Heller et al.*, 2001; *Surian*, 2002; *Brummer and Montgomery*, 2003; *Attal and Lavé*, 2006].

[50] The model results above unambiguously indicate that unraveling pebble abrasion rates from Sternberg fining coefficients derived from the downstream evolution of gravel bar sediment grain size cannot realistically be achieved, except in the very particular setting of a sediment source localized in the headwater of a river system without major ponding or aggradation along its course.

4.3. Deciphering the Information Contained in Sediments

[51] The primary control exerted by lithology on source grain-size distribution [*Attal and Lavé*, 2006] and on particle abrasion rate during fluvial transport raises an important issue with respect to provenance studies, detrital thermochronology and cosmogenic studies. These studies carried out on fluvial sands along rivers or on molassic series in sedimentary basins are used to document changes in erosion rate, tectonic activity or thrust activation through the exhumation of previously buried geologic units [e.g., *Vance et al.*, 2003; *Garzanti et al.*, 2007; *Wobus et al.*, 2003]. However, most of them are based on the assumption that the fluvial network system transmits without distortion the message that sources of sediment contain. Our experimental results show, however, that fluvial transport is far from neutral and represents a major filter that modifies the grain size distribution but also the lithologic proportion (and consequently the associated geochemical or mineralogical associated information) in each grain size class. In our simplified model (section 4.2.2) predicting the evolution of the sediment characteristics along a river fed with mixtures containing various amount of contrasted lithologies, the poorly resistant sediment particles supplied from hillslopes are quickly reduced in size and, as a result, the strongest lithology becomes quickly overrepresented in the bed load with respect to the weakest ones (Figure 13d). Conversely, in the fine fraction of the abrasion products (e.g., suspended load), the most resistant lithologies will be underrepresented downstream. This model prediction is consistent with the downstream evolution of the bed load lithologic composition of many river systems, in which the weakest lithologies vanish to the advantage of the strongest ones [e.g., *Parker*, 1991; *Attal and Lavé*, 2006; *Mezaki and Yabiku*, 1984]. It is essential to appreciate that a correct interpretation of the results provided by provenance methods relies on a good understanding of how the "fluvial transport filter" modifies the characteristics of the sediments between their point of origin and the location where they are measured.

[52] This experimental study suggests in addition that other variables such as flow stage and grain size control the fragmentation process and can thus affect the "fluvial transport filter." Conversely, such dependence could in theory be used to gain additional information on the transport conditions experienced by sediment from the analysis of detrital series along rivers and in sedimentary basins. Variations in roundness and lithologic content in particular could potentially reflect changes in transport conditions in the contributing area which could be associated with a large-scale change in relief and average slopes of the fluvial network or with a climate-induced change in river discharge.

4.4. Pebble Abrasion, Fluvial Incision, and the Development of River Long Profiles

[53] Because of the potentially important role of the bed load flux in determining river incision rates into bedrock [*Gilbert*, 1877; *Willgoose et al.*, 1991; *Howard et al.*, 1994; *Sklar and Dietrich*, 1998, 2004; *Whipple and Tucker*, 2002; *Cowie et al.*, 2008], our experimental results on the downstream evolution of bed load characteristics bring new constraints on the development of river long profiles. In particular, it has been hypothesized by *Whipple and Tucker* [2002] that downstream fining strongly influences the concavity of transport-limited river profiles. In their study, they suggested that the fining is such that transport-limited rivers (i.e., those whose gradient is primarily set by their need to transport the sediment load coming from upstream and adjacent hillslopes) should have a concavity index of $\sim$0.5 at steady state, i.e., close to the concavity index of steady state detachment-limited rivers. At high shear stress, commonly used transport laws give a sediment transport capacity scaling with fluvial shear stress to the power 3/2 [e.g., *Meyer-Peter and Müller*, 1948] and thus with cross-sectional stream power $\Omega = \rho_w g Q S$, where Q and S are the river discharge and slope respectively. If we assume that Q is a linear function of drainage area A and that the bed load

flux Q_b scales as a power law of drainage area ($Q_b \propto A^{\zeta}$), the concavity index of transport limited rivers is (1-ζ). An exponent $\zeta \sim 0.5$ would thus be required to produce a landscape eroded uniformly by transport-limited rivers with a concavity index of ~0.5.

[54] In a uniformly eroding landscape, bed load flux increases linearly with A in the absence of pebble abrasion, and thus $\zeta = 1$. To consider the role of abrasion on the downstream evolution of the bed load flux Q_b, let us consider the end-member examples presented in section 4.2.2 of a fluvial network incising into a landscape at a uniform rate (Appendix A and Figure 13). If pebbles are abraded at a constant rate along the fluvial network and in the case of monolithologic watersheds, the bed load flux converges asymptotically toward a value which is a function of the abrasion rate after a distance of ~$250/E_d$ (Figure 13c); the bed load fining ratio also reaches an asymptotic value after the same distance (Figure 13a). For poorly resistant lithologies, the downstream evolution of the bed load flux cannot be approximated by a power law (Figure 13c): beyond the point where the asymptotic value is reached, the bed load flux is constant. For the most resistant lithologies, because river lengths across actively eroded mountains rarely exceed 400 km, the asymptotic value is never reached (Figure 13c). In this case, the relationship between the bed load flux and drainage area can be approximated by a power law, but with an exponent close to 1. The importance of the most resistant lithology on the evolution of the bed load characteristics is emphasized when considering a mixture of poorly to highly resistant lithologies: even when it represents only 10% of the material supplied to the river, the most resistant lithology prevents the asymptotic value of bed load flux to be reached (Mixture 3; Figure 13c). Consequently, the downstream evolution of bed load flux for all three considered mixtures can also be reasonably fitted with a power law for distances up to 400 km (Figure 13c): the exponent ζ varies between 0.96 (one resistant lithology eroded at 0.2%/km) and 0.74 (Mixture 3 with only 10% of resistant lithology). An exponent $\zeta = 0.5$ can only be achieved when considering some specific mixture made of poorly (10%/km) to very poorly (100%/km) resistant lithologies but containing a few percent of moderately resistant pebbles to prevent the asymptotic behavior from being reached after a few tens of kilometers (result not displayed).

[55] In most natural cases, our simplified model of bed load evolution under the effect of pebble abrasion in a uniformly eroding landscape suggests that the intrinsic concavity index of purely transport-limited systems would rarely exceed 0.25 (corresponding to an exponent ζ of 0.75). Our preliminary results thus indicate that pure transport-limited models should produce river profiles with a lower concavity than detachment-limited models and therefore challenge *Whipple and Tucker*'s [2002] conclusion that most fluvial incision models in the literature would produce similar river profiles with a concavity index of ~0.5 at steady state. We have observed rivers with concavity indices of ~0.2 eroding the noncohesive conglomerates uplifted on the backlimb of the Siwaliks range at the front of the Himalayas: such rivers would represent a good natural example of transport-limited systems, that is, systems where eroding the bedrock does not require any additional work to the work needed for transporting the bed load, and may thus provide a counterexample to conventional scaling laws. On the other hand, *Johnson et al.* [2009] show evidence for transport-limited bedrock rivers exhibiting concavity indices of ~0.6 in the Henry Mountains of Utah. However, *Johnson et al.* [2009] highlight that, in these rivers, the coarse fraction of the bed load exerts a primary control on channel slope by setting the bed roughness and thus influencing transport capacity during floods. In addition, the sources of this coarse material are located in the headwaters and are not distributed along the rivers. Further modeling including more complexities (e.g., bed armoring, flood variability, feedbacks between bed roughness and transport capacity, role of fragmentation) is therefore required to provide definitive conclusions.

5. Conclusion

[56] In this study, we conducted series of experiments in two annular flumes in order to unravel the respective roles of the main factors controlling pebble abrasion rates and processes during fluvial transport. In those experiments, "abrasion" is the sum of "attrition," corresponding to the production of the finest abrasion products (<0.5 mm) which travel as suspended load, and "fragmentation" (breaking and splitting), associated with the production of angular fragments larger than 0.5 mm. Both processes are shown to be efficient in reducing particle size during fluvial transport. In our experiments, the amount of sediment controls the probability of impacts with the floor of the flume. For amounts exceeding ~30 to 70% of the amount required to cover the entire flume floor with pebbles and for a pebble velocity held constant, abrasion rates are independent of the amount of sediment. For low amounts of sediment, an abrasive bed condition (simulating impacts with bedrock or immobile pebbles) can produce abrasion rates up to 3.5 times higher than the abrasion rates produced solely by impacts between moving pebbles. For well-sorted material, particle size has a reduced influence on attrition rate but shows a clear positive control on fragment production rate, with large limestone pebbles ($D > 40$ mm) tending to promote fragment production. The rate of fragment production is highly variable, due to the stochasticity of the processes involved. For poorly sorted material, particle abrasion rate significantly decreases with increasing grain size. Mass loss by attrition appears to scale with particle velocity squared but additional experiments are required to confirm this trend for all particle sizes. The influence of velocity on fragment production rate is unclear, due to the high variability of fragment production rates, but high traveling velocities tend to promote fragmentation. Lithology exerts the strongest control on abrasion rates and processes. Differences in abrasion rates between lithologies can exceed 2 orders of magnitude and the ratio of mass loss by attrition to fragment production is highly lithology dependent. When compared to previously published experimental pebble abrasion rates, our results are similar for massive or resistant lithologies (quartzite, gneiss, granite, limestone) but up to one order of magnitude higher for rock types prone to breaking and splitting (schist, sandstone), our flume being the first one replicating the hydrodynamic conditions and highly energetic impacts prevailing during floods in mountain

rivers. Based on our experimental results, we extrapolate a preliminary generic relationship between pebble attrition rate and transport stage (τ^*/τ^*_c), where τ^* = fluvial Shields stress and τ^*_c = critical Shields stress for incipient pebble motion. This relationship predicts that attrition rates are independent of transport stage for $(\tau^*/\tau^*_c) \leq 3$ and increase linearly with transport stage beyond this value.

[57] Our simple model of evolution of sediment characteristics along a river flowing across a uniformly eroding landscape predicts that variations in the relative supply of sediments from contrasted lithologies lead to contrasted evolution of sediment characteristics but that the most resistant lithology exerts a strong control on sediment grain size and bed load flux. The model also predicts that bed load flux can be described as a power law of drainage area with an exponent varying between 0.75 and 1, providing that a permanent supply of sediment from a resistant rock type prevents the flux from reaching an asymptotic value. Such a result implies that the concavity index of river profiles produced using the transport-limited model of fluvial erosion would rarely exceed 0.25 and thus challenges the common view that the concavity indices of transport-limited and detachment-limited rivers should be indistinguishable, ~0.5. Our model results also emphasize that abrasion itself should not lead to a major downstream fining in most natural settings and that comparison of fining coefficients with experimental pebble abrasion rates is thus generally incorrect, unless the sediment is mostly composed of pebbles from highly erodible lithologies. We emphasize however that additional experiments on particle abrasion rates at low transport stage must be carried out to improve our modeling of low energy rivers (e.g., alluvial rivers). We also highlight that some processes which have not been fully investigated in this study (e.g., controls on fragment production rates, effect of differences in particle mobility for sediments including a wide range of particle sizes, role of weathering) must be integrated in the model in order to make realistic detailed predictions of the evolution of sediment characteristics along rivers. Such detailed predictions are essential if one wishes to efficiently model landscape evolution or interpret the results of thermochronologic, cosmogenic or provenance studies carried out on detrital sediments along fluvial networks or in sedimentary basins.

Appendix A: Description of the Model of Evolution of Sediment Characteristics Developed by *Attal and Lavé* [2006] and Used in This Study (Section 4.2.2)

[58] Following the approach proposed by *Attal and Lavé* [2006] for a simplified linear drainage geometry submitted to uniform erosion, we extend here the calculation to the particular case of the Hack's law with an exponent of 0.5, i.e., defined by the relation $L \propto A^{0.5}$ where A = drainage area and L distance from source. We assume that each rock fragment delivered from the hillslopes to the river network is reduced in size at a constant abrasion rate (equation (1)):

$$\frac{dV}{V} = -E_d dL_t \quad \text{or} \quad \frac{dD}{D} = -\frac{E_d}{3} dL_t, \tag{A1}$$

where E_d = particle abrasion rate, D and V = pebble diameter and volume respectively, and L_t = distance traveled by the particle. We also assume that the products of abrasion are fine materials that then transit as suspended load. If we now consider a uniform erosion rate ε and uniform sediment supply from the hillslopes and lateral tributaries with a unique fragment size D_0, we can write for any point along the main river stem for the total sediment flux:

$$Q_s(L) = \varepsilon A = \varepsilon \left(\frac{L}{c}\right)^2, \tag{A2}$$

for the bed load sediment flux:

$$Q_b(L) = \varepsilon \int_0^L e^{-E_d x} f_A(x) dx, \tag{A3}$$

for the mean pebble size:

$$\overline{D}(L) = D_0 \frac{\int_0^L e^{-E_d x} e^{-\frac{E_d}{3}x} f_A(x) dx}{\int_0^L e^{-E_d x} f_A(x) dx}, \tag{A4}$$

where $f_A(x)$ is the area density of the drainage located at a distance x from the considered point. For simplicity, we assume that such distribution can be approximated by $f_A(x) = \frac{2x}{c^2}$. Such distribution is compatible with Hack's law, since its integration between $x = 0$ (considered point) and $x = L$ (source of the river main stem) leads to

$$A = \int_0^L f_A(x) dx = \int_0^L \frac{2x}{c^2} dx = \left(\frac{L}{c}\right)^2. \tag{A5}$$

[59] Introducing above area density into (A3) and (A4) yields for the bed load sediment flux:

$$Q_b(L) = \frac{2\varepsilon}{c^2 E_d^2} \left(1 - (1 + E_d L) e^{-E_d L}\right), \tag{A6}$$

for the mean pebble size:

$$\overline{D}(L) = \frac{9}{16} D_0 \frac{\left(1 - \left(1 + \frac{4}{3} E_d L\right) e^{-\frac{4E_d}{3}L}\right)}{(1 - (1 + E_d L) e^{-E_d L})}. \tag{A7}$$

As for the linear drainage, an asymptotic behavior is rapidly reached both for the flux of bed load and the mean grain size at great distances from the river source or for high values of the particle abrasion rate E_d. The asymptotic value for the mean pebble size $D = 9/16\ D_0$ is independent of E_d (it is 3/4 D_0 for a linear drainage [*Attal and Lavé*, 2006]).

Notation

AIAS plateau refers to "plateau of Abrasion Independent of Amount of Sediment" (see section 3.1)

$\overline{xxx}$	refers to average of xxx
A	drainage area [L^2]
A_f	total area of the flume floor [L^2]

b coefficient [$L^{3-2\zeta}$ T^{-1}]
D particle diameter [L]
D_0 initial particle diameter [L]
D_{50} median sediment grain size [L]
E_d abrasion rate expressed in percent mass loss per unit traveled distance [L^{-1}]
${}^{att}E_d$ attrition rate expressed in percent mass loss per unit traveled distance [L^{-1}]
${}^{fr}E_d$ rate of fragment production expressed in percent mass loss per unit traveled distance [L^{-1}]
E_t abrasion rate expressed in percent mass loss per unit time [T^{-1}]
${}^{att}E_t$ attrition rate expressed in percent mass loss per unit time [T^{-1}]
g acceleration of gravity [LT^{-2}]
k coefficient in ${}^{att}E_d = k(U_p)^2$ [T^2L^{-3}]
L distance along river from source [L]
L_t distance traveled by particles [L]
m particle mass [M]
m_0 initial particle mass [M]
M_s mass of sediment introduced into the flume [M]
M_{sc} mass of sediment required to cover the flume's floor with close-packed pebbles [M]
n_p number of particles [dimensionless]
p packing density [dimensionless]
p_{cp} packing density corresponding to the full coverage of the floor of the flume with close-packed pebbles [dimensionless]
Q river discharge [L^3T^{-1}]
Q_b bed load flux [L^3T^{-1}]
Q_s total sediment flux [L^3T^{-1}]
r_m mean curvature radius of the flume [L]
S river slope [dimensionless]
S_e surface covered by pebbles [L^2]
U_{fl} mean fluid velocity across a flume section [LT^{-1}]
U_p mean particle traveling velocity [LT^{-1}]
u_p mean hop velocity [LT^{-1}]
w flume width [L]
dZ height difference between the top and the bottom of the vortex in the flume [L]
δ size reduction coefficient [L^{-1}]
ε landscape erosion rate [LT^{-1}]
θ river concavity index [dimensionless]
ρ_s sediment density [$L^{-3}M$]
ρ_w water density [$L^{-3}M$]
τ^* Shields stress [dimensionless]
τ^*_c critical Shields stress for particle entrainment [dimensionless]
ζ exponent in power relationship between Q_b and A [dimensionless]
Ω cross-sectional stream power [MT^{-3}]

[60] **Acknowledgments.** French programs "Action coup de pouce" and PNRH have financially supported this work. Part of this work has been done at the University of Edinburgh (the postdoctoral support of the first author was received through the University of Edinburgh and Patience Cowie's NERC research grant NE/B504165/1). We are extremely grateful to Rob Ferguson, Alex Densmore, Jens Turowski and an anonymous reviewer for thorough review and constructive comments on the different versions of the manuscript, including the initial "long version." We thank Greg Tucker and Alex Whittaker for providing constructive feedback on the last version of the manuscript. We sincerely thank Mark Naylor for providing valuable help for the statistical analysis of the results and Jean-Paul Masson for his immense contribution to the development of the experimental device.

References

Adams, J. (1978), Data for New Zealand pebble abrasion studies, *N. Z. J. Sci.*, *21*, 607–610.

Alberta Infrastructure and Transportation (2007), Alberta flood envelope curve analysis, report, , Edmonton, AB, Canada. (Available at http://www.transportation.alberta.ca/Content/docType30/Production/fldenvcurv.pdf)

Attal, M. (2003), Erosion des galets des rivières de montagne au cours du transport fluvial: Étude expérimentale et application aux réseaux hydrographiques d'orogènes actifs, Ph.D. thesis, 279 pp., Univ. J. Fourier, Grenoble, France.

Attal, M., and J. Lavé (2006), Changes of bedload characteristics along the Marsyandi River (central Nepal): Implications for understanding hillslope sediment supply, sediment load evolution along fluvial networks, and denudation in active orogenic belts, *Spec. Pap. Geol. Soc. Am.*, *398*, 143–171, doi:10.1130/2006.2398(09).

Attal, M., J. Lavé, and J.-P. Masson (2006), New facility to study river erosion processes, *J. Hydrol. Eng.*, *132*(6), 624–628, doi:10.1061/(ASCE)0733-9429(2006)132:6(624).

Bradley, W. C. (1970), Effect of weathering on abrasion of granitic gravel, Colorado River (Texas), *Geol. Soc. Am. Bull.*, *81*, 61–80, doi:10.1130/0016-7606(1970)81[61:EOWOAO]2.0.CO;2.

Brewer, P. A., and J. Lewin (1993), In-transport modification of alluvial sediment: Field evidence and laboratory experiments, *Spec. Publ. Int. Assoc. Sedimentol.*, *17*, 23–35.

Brierley, G. J., and E. J. Hickin (1985), The downstream gradation of particle sizes in the Squamish River, British Colombia, *Earth Surf. Processes Landforms*, *10*, 597–606, doi:10.1002/esp.3290100607.

Brummer, C. J., and D. R. Montgomery (2003), Downstream coarsening in headwater channels, *Water Resour. Res.*, *39*(10), 1294, doi:10.1029/2003WR001981.

Bullows, W. L. (1939), Notes on the artificial production of pebbles by "barreling," *Quarry Managers J.*, *21*, 377–397.

Burbank, D. W., J. Leland, E. Fielding, R. S. Anderson, N. Brozovic, M. R. Reid, and C. Duncan (1996), Bedrock incision, rock uplift and threshold hillslopes in the northwestern Himalayas, *Nature*, *379*, 505–510, doi:10.1038/379505a0.

Burnham, K. P., and D. R. Anderson (2002), *Model Selection and Multimodel Inference*, 496 pp., Springer, New York.

Chang, H. H. (1988), *Fluvial Processes in River Engineering*, 425 pp., John Wiley, New York.

Constantine, C. R., J. F. Mount, and J. L. Florsheim (2003), The effects of longitudinal differences in gravel mobility on the downstream fining pattern in the Cosumnes River, California, *J. Geol.*, *111*, 233–241, doi:10.1086/345844.

Cowie, P. A., A. C. Whittaker, M. Attal, G. P. Roberts, G. E. Tucker, and A. Ganas (2008), New constraints on sediment-flux-dependent river incision: Implications for extracting tectonic signals from river profiles, *Geology*, *36*(7), 535–538, doi:10.1130/G24681A.1.

Daubrée, A. (1879), *Etudes Synthétiques de Géologie Expérimentale*, Dunod, Paris.

Ferguson, R., T. Hoey, S. Wathen, and A. Werritty (1996), Field evidence for rapid downstream fining of river gravel through selective transport, *Geology*, *24*(2), 179–182, doi:10.1130/0091-7613(1996)024<0179:FEFRDF>2.3.CO;2.

Finnegan, N. J., G. Roe, D. R. Montgomery, and B. Hallet (2005), Controls on the channel width of rivers: Implications for modeling fluvial incision of bedrock, *Geology*, *33*, 229–232, doi:10.1130/G21171.1.

Garzanti, E., G. Vezzoli, S. Andò, J. Lavé, M. Attal, C. France-Lanord, and P. DeCelles (2007), Quantifying sand provenance and erosion (Marsyandi River, Nepal Himalaya), *Earth Planet. Sci. Lett.*, *258*(3–4), 500–515, doi:10.1016/j.epsl.2007.04.010.

Gilbert, G. K. (1877), *Report on the Geology of the Henry Mountains: Geographical and Geological Survey of the Rocky Mountain Region*, 160 pp., U.S. Gov. Print. Off., Washington, D. C.

Hack, J. T. (1957), Studies of longitudinal profiles in Virginia and Maryland, *U.S. Geol. Surv. Prof. Pap., 294-B*, 97 pp.

Heller, P. L., P. E. Beland, N. F. Humphrey, S. K. Konrad, R. M. Lynds, M. E. McMillan, K. E. Valentine, Y. A. Widman, and D. J. Furbish (2001), Paradox of downstream fining and weathering-rind formation in the lower Hoh River, Olympic Peninsula, Washington, *Geology*, *29*, 971–974, doi:10.1130/0091-7613(2001)029<0971:PODFAW>2.0.CO;2.

Howard, A. D., W. E. Dietrich, and M. A. Seidl (1994), Modeling fluvial erosion on regional to continental scales, *J. Geophys. Res.*, *99*, 13,971–13,986, doi:10.1029/94JB00744.

Ikeda, S., G. Parker, and Y. Kimura (1988), Stable width and depth of straight gravel rivers with heterogeneous bed materials, *Water Resour. Res.*, *24*(5), 713–722, doi:10.1029/WR024i005p00713.

Johnson, J. P. L., K. X. Whipple, L. S. Sklar, and T. C. Hanks (2009), Transport slopes, sediment cover, and bedrock channel incision in the

Henry Mountains, Utah, *J. Geophys. Res.*, *114*, F02014, doi:10.1029/2007JF000862.

Jones, L. S., and N. F. Humphrey (1997), Weathering-controlled erosion in a coarse-grained, meandering reach of the Rio Grande: Implications for the rock record, *Geol. Soc. Am. Bull.*, *109*, 1080–1088, doi:10.1130/0016-7606(1997)109<1080:WCAIAC>2.3.CO;2.

Knighton, A. D. (1982), Longitudinal changes in the size and shape of stream bed material: Evidence of variable transport conditions, *Catena*, *9*, 25–34, doi:10.1016/S0341-8162(82)80003-9.

Kodama, Y. (1994a), Downstream changes in the lithology and grain size of fluvial gravels, the Watarase River, Japan: Evidence of the role of erosion in downstream fining, *J. Sediment. Res., Sect. A*, *64*, 68–75.

Kodama, Y. (1994b), Experimental study of erosion and its role in producing downstream fining in gravel-bed rivers, *J. Sediment. Res., Sect. A*, *64*, 76–85.

Krumbein, W. C. (1941), The effects of abrasion on the size, shape and roundness of rock fragments, *J. Geol.*, *49*, 482–520, doi:10.1086/624985.

Kuenen, P. H. (1956), Experimental erosion of pebbles: 2. Rolling by current, *J. Geol.*, *64*, 336–368, doi:10.1086/626370.

Kukal, Z. (ed.) (1990), The Rate of Geological Processes, *Earth Sci. Rev.*, *28*, 284 pp.

Leopold, L. B., and T. Maddock (1953), The hydraulic geometry of stream channels and some physiographic implications, *U.S. Geol. Surv. Prof. Pap.*, *252*.

Lewin, J., and P. A. Brewer (2002), Laboratory simulation of clast abrasion, *Earth Surf. Processes Landforms*, *27*, 145–164, doi:10.1002/esp.306.

Meyer-Peter, E., and R. Müller (1948), Formulas for bed-load transport, paper presented at 2nd Meeting, Int. Assoc. for Hydraul. Res., Delft, Netherlands.

Mezaki, S., and M. Yabiku (1984), Channel morphology of the Kali Gandaki and the Narayani rivers in central Nepal, *J. Nepal Geol. Soc.*, *4*, 161–176.

Mikos, M. (1994), The downstream fining of gravel-bed sediments in the Alpine Rhine River, in *Dynamics and Geomorphology of Mountain Rivers*, edited by P. Ergenzinger and K.H. Schmidt, pp. 93–108, Springer, Berlin.

Mikos, M., and M. N. R. Jaeggi (1995), Experiments on motion of sediment mixtures in a tumbling mill to study fluvial erosion, *J. Hydraul. Res.*, *33*, 751–772.

Montgomery, D. R., and K. B. Gran (2001), Downstream variations in the width of bedrock channels, *Water Resour. Res.*, *37*, 1841–1846, doi:10.1029/2000WR900393.

Moussavi-Harami, R., A. Mahboubi, and M. Khanehbad (2004), Analysis of controls on downstream fining along three gravel-bed rivers in the Band-e-Golestan drainage basin NE Iran, *Geomorphology*, *61*, 143–153, doi:10.1016/j.geomorph.2003.12.005.

Niño, Y., and M. García (1994), Gravel saltation: 2. Modeling, *Water Resour. Res.*, *30*(6), 1915–1924, doi:10.1029/94WR00534.

Niño, Y., M. García, and L. Ayala (1994), Gravel saltation: 1. Experiments, *Water Resour. Res.*, *30*(6), 1907–1914, doi:10.1029/94WR00533.

Paola, C., G. Parker, R. Seal, S. K. Sinha, J. B. Southard, and P. R. Wilcock (1992), Downstream fining by selective deposition in a laboratory flume, *Science*, *258*, 1757–1760, doi:10.1126/science.258.5089.1757.

Parker, G. (1991), Selective sorting and erosion of river gravel, II: Applications, *J. Hydrol. Eng.*, *117*(2), 150–171.

Pearce, T. H. (1971), Short distance fluvial rounding of volcanic detritus, *J. Sediment. Petrol.*, *41*, 1069–1072.

Schoklitsch, A. (1933), Über die verkleinerung der geschiebe in flussläufen, *Sitzungsber. Akad. Wiss. Wien, IIa*, *142*, 343–366.

Shaw, J., and R. Kellerhals (1982), The composition of recent alluvial gravels in Alberta river beds, *Bull. 41*, 151 pp., Alberta Geol. Surv., Edmonton, AB, Canada.

Sklar, L., and W. E. Dietrich (1998), River longitudinal profiles and bedrock incision models: Stream power and the influence of sediment supply, in *Rivers Over Rock: Fluvial Processes in Bedrock Channels*, *Geophys. Monogr. Ser.*, vol. 107, edited by K. J. Tinkler and E. E. Wohl, pp. 237–260, AGU, Washington, D. C.

Sklar, L. S., and W. E. Dietrich (2001), Sediment and rock strength controls on river incision into bedrock, *Geol. Soc. Am. Bull.*, *29*, 1087–1090.

Sklar, L. S., and W. E. Dietrich (2004), A mechanistic model for river incision into bedrock by saltating bed load, *Water Resour. Res.*, *40*, W06301, doi:10.1029/2003WR002496.

Sklar, L. S., W. E. Dietrich, E. Foufoula-Georgiou, B. Lashermes, and D. Bellugi (2006), Do gravel bed river size distributions record channel network structure?, *Water Resour. Res.*, *42*, W06D18, doi:10.1029/2006WR005035.

Sternberg, H. (1875), Untersuchungen über längen- und querprofile geschiebführender flüsse, *Z. Bauwes.*, *25*, 483–506.

Surian, N. (2002), Downstream variation in grain size along an Alpine river: Analysis of controls and processes, *Geomorphology*, *43*, 137–149, doi:10.1016/S0169-555X(01)00127-1.

Vance, D., M. Bickle, S. Ivy-Ochs, and P. W. Kubik (2003), Erosion and exhumation in the Himalaya from cosmogenic isotope inventories of river sediments, *Earth Planet. Sci. Lett.*, *206*(3–4), 273–288, doi:10.1016/S0012-821X(02)01102-0.

Wentworth, C. K. (1919), A laboratory and field study of cobble abrasion, *J. Geol.*, *27*, 507–522, doi:10.1086/622676.

Whipple, K. X., and G. E. Tucker (2002), Implications of sediment-flux-dependent river incision models for landscape evolution, *J. Geophys. Res.*, *107*(B2), 2039, doi:10.1029/2000JB000044.

Whipple, K. X., E. Kirby, and S. Brocklehurst (1999), Geomorphic limits to climatically induced increases in topography relief, *Nature*, *401*, 39–43, doi:10.1038/43375.

Whittaker, A. C., P. A. Cowie, M. Attal, G. E. Tucker, and G. P. Roberts (2007), Contrasting transient and steady-state rivers crossing active normal faults: New field observations from the central Apennines, Italy, *Basin Res.*, *19*, 529–556, doi:10.1111/j.1365-2117.2007.00337.x.

Willgoose, G., R. L. Bras, and J. Rodriguez-Iturbe (1991), A coupled channel network growth and hillslope evolution model: 1. Theory, *Water Resour. Res.*, *27*, 1671–1684, doi:10.1029/91WR00935.

Wobus, C. W., K. V. Hodges, and K. X. Whipple (2003), Has focused denudation sustained active thrusting at the Himalayan topographic front?, *Geology*, *31*(10), 861–864, doi:10.1130/G19730.1.

M. Attal, School of GeoSciences, University of Edinburgh, Drummond St., Edinburgh EH8 9XP, UK. (mikael.attal@ed.ac.uk)

J. Lavé, Centre de Recherches Pétrographiques et Géochimiques, F-54501 Nancy, France.